RESOURCE ARTICLE

Prox1 dynamically regulates downstream targets and chromatin accessibility during venous to lymphatic endothelial cell transdifferentiation in the embryo

Lin Grimm[1,2,3,*], Elizabeth Mason[1,2*], Stefanie Dudczig[1,2], Jan Kazenwadel [4,5], Tyrone Chen[1,2], Oliver Yu[1,2], Neil I. Bower[3], Scott Paterson[1,2,3], Kazuhide Okuda[1,2], Maria Rondon Galeano[1,2], Sakurako Kobayashi[1,2], Anne Senabouth[3,4], Anne K. Lagendijk[3], Joseph Powell[3,6,7,8], Kelly A. Smith[9], Natasha L. Harvey[4,5], Katarzyna Koltowska[10] and Benjamin M. Hogan[1,2,3,9 #].

[1] Organogenesis and Cancer Program, Peter MacCallum Cancer Centre, Melbourne, VIC 3000, Australia.
[2] Sir Peter MacCallum Department of Oncology, University of Melbourne, Melbourne, VIC 3000, Australia.
[3] Division of Genomics of Development and Disease, Institute for Molecular Bioscience, The University of Queensland, St Lucia, Brisbane, Queensland 4072, Australia.
[4] Centre for Cancer Biology, University of South Australia and SA Pathology, Adelaide, South Australia, 5001, Australia.
[5] SA Pathology, Adelaide, South Australia, 5001, Australia.
[6] Garvan Institute of Medical Research, 384 Victoria Street, Darlinghurst, Sydney, 2010, Australia.
[7] School of Medical Sciences, 18 High Street, University of New South Wales, Kensington, Sydney, Australia.
[8] Garvan-Weizmann Centre for Cellular Genomics, Garvan Institute of Medical Research, 384 Victoria Street, Darlinghurst, Sydney, 2010, Australia.
[9] Department of Anatomy and Physiology, University of Melbourne, Melbourne, VIC 3000, Australia.
[10] Department of Immunology, Genetics and Pathology, Uppsala University, Uppsala, Sweden.

[#] *Author for Correspondence:*

Professor Ben Hogan
Organogenesis and Cancer Program,
Peter MacCallum Cancer Centre,
Melbourne, VIC 3000, Australia
E-mail: ben.hogan@petermac.org

Keywords: Lymphatics, Lymphangiogenesis, Prox1, Single cell, RNA Seq, ATAC seq.
Summary: 149 words
Main Text: 4378 words

During development, lymphatic vasculature forms as a second, distinct vascular network derived from blood vessels. Transdifferentiation of venous into lymphatic endothelial cells (LECs) is the first step in this process. Specification, transdifferentiation and maintenance of LEC fate requires the transcription factor Prox1 but downstream mechanisms and markers remain to be described in full. We present a single cell transcriptomic atlas of lymphangiogenesis in zebrafish revealing new markers and hallmarks of LEC differentiation. We further profile single cell transcriptomic and chromatin accessibility changes in Prox1 mutants. This work reveals dynamic, multifaceted roles for Prox1 that include blocking blood vascular and hematopoietic fate and up-regulating essential factors for lymphatic development. We reveal that Prox1 controls chromatin state and evidence for Prox1-independent regulation of early LEC differentiation. This work thus provides new insights and a detailed resource for further understanding an enigmatic developmental process that is central in pathological lymphangiogenesis in disease.

Introduction

Lymphatic vasculature plays crucial physiological roles that include the drainage of interstitial fluids, trafficking of immune cells and drainage of dietary lipids. The formation of new lymphatic vessels from pre-existing vessels (lymphangiogenesis) occurs in both development and disease. Signalling through Vegfr3 (Flt4) can be triggered by Vegfc or Vegfd and drives lymphangiogenesis in settings as diverse as development, cancer metastasis, inflammation and ocular disease [1]. In the embryo, lymphangiogenesis begins when the first LEC progenitors depart the cardinal veins (CVs) from E9.5 in mice and 32 hours post fertilisation (hpf) in zebrafish [2]. Vegfc-Flt4 signalling drives LEC progenitor sprouting but also up-regulates Prox1 expression in both zebrafish and mice [3-7]. The transcription factor Prox1 acts as the master regulator of LEC fate [8] and is exclusively expressed in developing LECs in early embryonic vasculature. Loss of Prox1 (Prox1a and Prox1b in zebrafish) leads to a loss of developing lymphatic vessels [4,9]. Following departure from the CV, LEC progenitors go on to colonise embryonic tissues and organs and remodel to form functional lymphatic vessels [10]. While at later stages in mammals there are contributions of LECs from non-venous origins, early embryonic lymphanigogenesis occurs chiefly from the CVs [11-17]. In mice, both the earliest stages of LEC progenitor sprouting from CVs and maintenance of LEC fate in stable lymphatics are dependent on the function of Prox1 [9,18].

77

78 Despite over two decades of study of this enigmatic developmental process, the
79 transcriptomic changes that occur as embryonic venous endothelial cells (VECs)
80 transdifferentiate into LEC progenitors, and further differentiate into mature lymphatics,
81 have not been transcriptionally profiled *in vivo*. In the absence of Prox1 in conditional
82 knockout mice, LECs have been shown to lose the expression of some LEC markers and to gain
83 expression of some blood vascular endothelial cell (BEC) markers[18]. Prox1 is known to
84 autoregulate its own expression and to also regulate Flt4 expression in a positive regulatory
85 loop during early development[7]. Yet how Prox1 controls the transcriptome during LEC
86 specification, differentiation and maintenance has not been described. This is in part because
87 of the technical challenge of accessing early mouse endothelial cells in wildtype and mutant
88 embryos, a problem that is not limiting when using the zebrafish embryo.

89

90 As recent studies have demonstrated highly conserved expression and function of Prox1
91 homologues in zebrafish[4,6,19,20], we here took advantage of the accessibility of the zebrafish
92 embryo to examine developmental lymphangiogenesis using single cell transcriptomics. We
93 further analysed zebrafish zygotic *prox1a* mutants with single cell RNA sequencing and single
94 cell ATAC sequencing, as well as maternal-zygotic double *prox1a/prox1b* mutant (null Prox1
95 mutants) vasculature with single cell RNA sequencing. Overall, we reveal that embryonic
96 lymphangiogenesis is a highly conserved process involving dynamic and discrete Prox1-
97 dependent and independent mechanisms. We provide a resource of new markers of VEC-LEC
98 transdifferentiation, differentiating and mature cell types and we demonstrate the utility of
99 this resource to identify a new Prox1-dependent regulator of lymphangiogenesis, the
100 transmembrane protein Tspan18.

101

102 **Results**

103 **A single cell RNA-seq atlas of embryonic lymphangiogenesis**

104 Zebrafish secondary angiogenesis occurs when Prox1-positive LECs and VECs both sprout
105 from the cardinal vein (CV) in the trunk or the head in a progressive process between ~32 and
106 ~48hpf. In the trunk, sprouting LECs migrate dorsally and invest the horizontal myoseptum,
107 where they form a transient pool of parachordal LECs (PLs) from approximately 48hpf[21,22]. In
108 craniofacial regions of the embryo, LECs sprout from the CVs at several locations[23,24]. After

109 this, LECs throughout the embryo proliferate and migrate extensively (between ~56hpf-
110 80hpf) to colonise new regions and tissues[24-27]. In the trunk, LECs anastomose to form the
111 first lymphatic vessels at around 4 days post fertilisation; forming the thoracic duct (TD),
112 dorsal longitudinal lymphatic vessels (DLLVs) and intersegmental lymphatic vessels (ISLVs). In
113 craniofacial regions, they assemble from disparate sources into lateral (LFL), medial (MFL),
114 otolithic lymphatic vessels (OLV) and lymphatic branchial arches (LBA), as well as forming a
115 lymphatic loop (LL) in the head that will later give rise to a unique mural LEC population in the
116 brain (muLECs, also known as FGPs or brain LECs)[28-30]. By 5dpf, major lymphatics in the
117 craniofacial and trunk regions of the embryo are functional and drain dyes and fluids
118 deposited in the peripheral tissues[22,31].
119
120 To profile stages of development spanning key steps in lymphatic differentiation, we selected:
121 40hpf, when specification and initial sprouting of LECs are occurring; 3dpf, when immature
122 LECs are migrating through the embryo; 4dpf when LECs are assembling into vessels; and 5dpf
123 when lymphatics are functional and maturing[32] (**Fig. 1a**). We used transgenic zebrafish strains
124 that specifically labelled embryonic vasculature to allow for fluorescence activated cell sorting
125 (FACS, full details in methods). We dissociated whole transgenic embryos and FAC sorted
126 endothelial cells, for profiling on the 10X Chromium scRNA-seq platform. We sequenced
127 35,634 cells across 3 runs, then merged and normalised the data[33,34], filtering low-quality
128 libraries (**Extended data Fig 1a**). To define the cellular identity of each cluster, we
129 systematically evaluated the expression of known markers summarised in **Extended data**
130 **Table 1a**. We identified 9,771 lymphatic and venous endothelial cells that comprise our single
131 cell atlas of lymphangiogenesis (**Fig 1b**, **Extended data Fig 1b-c**).
132
133 This dataset is displayed[35] as a UMAP in **Fig 1b** coloured according to developmental stage
134 and cell phenotype, with venous (VEC) to lymphatic (LEC) trajectory of differentiation
135 confirmed by RNA-velocity analysis[36]. Comparison of cells at 40hpf with later stages revealed
136 that the earlier populations are transcriptionally distinct from VECs and LECs at 3, 4 and 5dpf.
137 Notably, the 40hpf "VEC preLEC" cluster contained both *prox1a+* and *prox1a-* cells forming a
138 single population rather than discrete clusters. This indicates that LECs are not
139 transcriptionally distinct from VECs at 40hpf, suggesting early *prox1a+* cells are specified but
140 not yet differentiated LECs (**Fig 1c**)[4]. We identified 3 main classes of LECs at 3, 4 and 5dpf:

141 muLECs (1511 cells) marked by expression of *osr2*[28], canonical LECs marked by expression of
142 *cdh6* (2669 cells), and a smaller sub-population of LECs expressing low levels of *prox1a*
143 (LEC_low_prox1a, 310 cells) (**Fig 1c**, **Extended data Fig 1d-e**). To define markers of
144 differentiating canonical LECs at each developmental stage, we applied differential
145 expression (DE) analysis (**Extended data Table 1b**,). This analysis not only captured known
146 LEC markers including *prox1a, angpt2a, tbx1* and *cldn11b*, but also uncovered new genes
147 commonly expressed in canonical LECs across all developmental stages including *grp156,*
148 *hapln3, cdh6* and *tspan18a* (**Fig 1d, Extended data Fig 1f**). We extended this approach and
149 evaluated global differences between all canonical LECs and all VECs (n=1240 genes,
150 **Extended data table 1c**). GO analysis[37] confirmed the association of biological processes
151 known to be associated with lymphatics with genes upregulated in LEC (n=752 LEC gene set),
152 these terms included "lymphangiogenesis", "glycolytic process", "lymph vessel development"
153 and "ameboidal-type cell migration" (**Fig 1e**, **Extended data Table 1d**).

154 To provide further confidence in the specificity of the new LEC markers defined by this scRNA-
155 seq resource, we used DE analysis to defined cluster specific gene expression. We noted that
156 this analysis suggested higher expression of the well-known marker *lyve1b* in muLECs than in
157 LECs, which we validated by examining expression levels of *lyve1b* using the established
158 transgenic line *Tg(lyve1b:DsRed2)* (heat map in **Fig 2a**). We further identified expression of
159 the known kidney epithelial solute transporter *slc7a7a* as uniquely expressed in muLEC cells
160 and *fabp11a* as a canonical LEC and VEC marker excluded from muLECs. We generated both
161 new *slc7a7a*–Citrine and a *fabp11a-Citrine* BAC transgenic strains, which confirmed the
162 restricted muLEC and vascular expression patterns and further validated our scSeq atlas of
163 lymphatic differentiation (**Fig 2b-c**). Overall, this atlas therefore identifies n=752 specific
164 markers of lymphangiogenesis, the majority of which are new markers, representing new
165 candidate regulators and spanning four developmental stages.

166

167 **Prox1 maintains lymphatic endothelial cell identity by repressing blood vascular fate and**
168 **promoting lymphatic vascular fate at the level of the transcriptome**

169 Prox1 is both necessary and sufficient to drive VEC to LEC trans-differentiation in mammals
170 and this is proposed to occur by Prox1 simultaneously initiating LEC fate and repressing the
171 VEC fate program[8,18]. Prox1 expression is also necessary for the maintenance of LEC identity
172 during development[18,38,39]. Despite the role for Prox1 being well-studied in mouse models,
173 the transcriptomic program controlled by Prox1 *in vivo* has never been profiled. Zebrafish
174 *prox1a* zygotic and maternal zygotic mutants have been previously described[4,20]. The zygotic
175 mutants retain maternal deposition of *prox1a* in the oocyte, sufficient to drive normal PL
176 formation, LEC migration to the horizontal myoseptum (HM) and initial assembly of
177 lymphatics by 4dpf[4,19], however mutants have a reduction in total LEC numbers throughout
178 the face and trunk[4]. When the maternal contribution of *prox1a* is removed, lymphatic
179 development is more severely impaired[4]. We hypothesised that the zygotic mutants which
180 form lymphatic vessels, likely have abnormal vessel identity in the absence of zygotic Prox1.
181 Thus, we first addressed the question of how Prox1 regulates lymphatic differentiation by
182 taking advantage of this unique model. We applied scRNA-seq to endothelial cells FAC sorted
183 from *Zprox1a*$^{-/-}$ mutants[20] and WT sibling zebrafish at 4dpf, during lymphatic vessel assembly
184 (n=8075 cells, **Extended data Fig 2a**, **Extended data Table 2a**). Cluster analysis revealed 3
185 populations of LECs (n=2068) and a single population of VECs (n=1051) comprising both
186 mutant and wild type cells, and perhaps most striking, a single population of mutant cells
187 (n=484) transcriptionally similar to VECs, marked by the expression of *aqp1a.1* (**Fig 3a-b**,
188 **Extended data Figs 2b-e**). All three LEC clusters (LEC, LEC_S1, LEC_S2) showed graded
189 expression of lymphatic markers *prox1a*, *cldn11b*, *cdh6* and *angpt2a*, such that "LEC" most
190 closely resembles canonical LECs from our WT atlas. LEC_S1 and S2 represent alternative LEC
191 sub-types with different proliferative potential based on S-phase occupancy and cell cycle
192 marker *mki67* (**Fig 3b**, **Extended data Fig 2e**). The expression of *prox1a* was lowest in the
193 more proliferative LEC_S1 cells, and highest in the less proliferative LEC_S2 (**Fig 3c**). RNA-
194 velocity analysis suggested a trajectory between the mutant cluster and the LEC cluster.
195 Taken together, these findings suggest that the mutant specific cluster sits on a trajectory
196 between LEC and VEC fate, representing cells either failing to fully differentiate from VEC to
197 LEC or LECs undergoing dedifferentiation.
198
199 To survey how Prox1 maintains normal LEC differentiation, we performed DE analysis
200 comparing the mutant cluster with WT LEC (**Fig 3f**, **Extended data Table 2b**). Overall, a much

201 larger set of genes were downregulated than upregulated in the mutant cluster (n=1034 vs
202 n=294) with almost half of the most downregulated genes (AvLogFC) highly enriched for LEC
203 markers (eg. *tbx1*, *cdh6*, *cldn11b*). Of the upregulated genes, almost 75% were VEC markers
204 (eg. *sox7*, *kdrl*, *cdh5*) and again this was enriched in the most highly upregulated genes (**Fig**
205 **3f, Extended data Fig 2f**). Comparing the change in gene expression between wildtype LEC
206 cluster and VEC cluster, with the change between wildtype LEC and mutant cluster, we found
207 striking concordance suggesting the mutant cluster is shifted along a LEC fate to VEC fate
208 trajectory (**Fig 3g**). Overall, there is a simultaneous loss of lymphatic fate and re-acquisition
209 of blood vascular gene expression, consistent with work in mouse and with Prox1 function
210 being highly conserved between vertebrates. To validate these observations, we used
211 confocal imaging of Z*prox1a*$^{-/-}$ mutants and observed upregulation of blood vascular markers
212 *cdh5* (**Fig 3h-i, Extended data Fig 3a,c**) and *kdrl* (**Fig 3j-k, Extended data Fig 3d-g**) in *lyve1b*-
213 positive lymphatics vessels. We saw a coincident reduction in the expression of *lyve1b* in
214 these vessels (**Extended data Fig3b).** Interestingly, the difference in *kdrl* levels (relative
215 intensity) in lymphatics between mutants and wildtype was more significant at 5dpf than
216 4dpf, suggesting that progressive dedifferentiation may be occurring in the mutant (**Fig 3k**).
217 This single cell profile thus demonstrates that Prox1 alone is sufficient to maintain LEC fate
218 and identifies the gene expression maintained by Prox1 in the differentiating lymphatic
219 vasculature.
220

221 **Prox1 mutant cells that fail to differentiate, display a unique, immature chromatin**
222 **signature**

223 At the level of gene expression, Prox1 function is essential for VEC to LEC differentiation,
224 however it is unknown if Prox1 controls chromatin accessibility during this process. Thus, we
225 next profiled *Zprox1a*$^{-/-}$ mutants at 4dpf during vessel assembly using single nuclei (sn) ATAC-
226 seq (n=3,731 nuclei, **Extended data Fig 4a, Extended data Table 3a**). Cluster analysis (**Fig 4a**)
227 and overall accessibility of key markers (**Fig 4b**) identified similar populations to the scRNA-
228 seq profiling: canonical LEC (LEC_01 n=114 nuclei, LEC_02 n=213 nuclei) and VEC (VEC_01
229 n=157 nuclei) clusters, and a small but discrete population comprised almost entirely of
230 mutant cells (Mutant Cluster n=47 nuclei). Notably, we found that there was almost no
231 contribution of mutant cells to the LEC clusters (**Fig 4a** lower bar plot), indicating a loss of fate
232 when cell identity is determined at the level of chromatin state **(Extended data Fig 4b-e)**. To

233 validate the utility of this dataset, we assessed concordance between gene expression and
234 chromatin accessibility in WT LECs and WT VECs (**Fig 4c**). DA (differential accessibility) analysis
235 revealed the more accessible regions in the LEC clusters were associated with LEC genes
236 identified in our atlas, and the less accessible regions with VEC genes (**Fig 4c, Extended data**
237 **table 3b**). These regions were enriched for motifs of lymphatic-specific transcription factors
238 including Mafa, Mafb, and the Tbx family **(Extended data table 3c)**. Several markers of LEC
239 and VEC identity demonstrated overall concordance between chromatin accessibility (gene
240 score) and gene expression (**Figure 4d**), including DA regions in *cdh6* (**Fig 4d and e**) and *cdh5*
241 (**Fig 4d and f**). This was consistent with observations in the scRNA-seq data, providing further
242 evidence that the Prox1a deficient cells assembling into fragmented lymphatic vessels are not
243 differentiated LECs.
244
245 Given that cells in the mutant specific cluster lacking Prox1 demonstrate loss of lymphatic
246 gene expression and acquisition of blood vascular gene expression, we expected chromatin
247 accessibility to change in an equally coordinated manner. However, analysis of accessibility
248 at individual genes (gene score) for the Mutant Cluster revealed changes inconsistent with a
249 simple fate shift (**Fig 5a-b, Extended data Fig 4f**). Notably, at the level of individual peaks we
250 found that 1726 peaks displayed a striking increase in accessibility compared to WT LEC and
251 1794 peaks an increase compared with WT VEC (**Fig 5b**, **Extended data tables 4a-b**). Of these,
252 431 were common peaks identifying more accessible chromatin regions in the mutant cluster
253 than in either WT LEC or WT VEC (**Fig 5b**). This suggests that some regions of chromatin open
254 up more than usual during LEC or VEC differentiation in the absence of Prox1. Most genes
255 with increased accessibility did not show a concurrent increase in gene expression, and we
256 observed no pattern or trend in expression overall (**Fig 5c**). These more open regions were
257 enriched for motifs of early acting transcription factors involved in embryonic vasculogenesis
258 and haematopoiesis, including Erg, Etv2, Ets1, Fli1 and Spi1/Pu.1 (**Fig 5d**, **Extended data table**
259 **4c**). We take this to suggest that in the absence of Prox1, transcription factors that normally
260 drive earlier transitions during vasculogenesis and haematopoiesis activate a unique
261 developmental chromatin signature. This demonstrates that Prox1 coordinates the correct
262 accessibility of the chromatin while maintaining LEC fate in endothelial cells. Furthermore, we
263 note that a large number of the genes with increased chromatin accessibility are known

264 regulators of lymphangiogenesis and so this increased accessibility may be a sensitive way to
265 identify key regulatory genes (**Extended data table 4c**).
266
267 **Prox1 is primarily a negative regulator of blood and blood vascular fate during the**
268 **specification of LEC fate and VEC-LEC transdifferentiation**
269 While the above data identifies the role of Prox1 at stages when it is maintaining LEC identity
270 in assembling LECs, Prox1 is essential for the very earliest decision made when a VEC becomes
271 specified to develop into a LEC[9]. To ask how Prox1 controls the earliest stages of venous to
272 lymphatic transdifferentiation, we first needed to generate a complete Prox1 loss of function
273 model in zebrafish. We generated *prox1a*$^{+/-}$, *prox1b*$^{+/-}$ double heterozygous animals (lacking
274 both Prox1 homologues) and then used germline transplantation approaches to produce
275 animals carrying a double mutant germline (**Extended data Fig 5a-b**). Genetic crossing of
276 these animals generated embryos that were maternal zygotic (MZ) *MZprox1a*$^{-/-}$, *MZprox1b*$^{-/-}$
277 mutant zebrafish completely lacking *prox1a/b* transcript expression or maternal deposition
278 (**Fig 6a-b; Extended data Fig 5c**). A quantitative phenotypic analysis revealed double MZ
279 mutants show a severe reduction of facial lymphatics and a near complete loss of lymphatic
280 vessels in the trunk by 4dpf (**Fig 6d-e**, **Extended data Fig 5f-h**) [4]. Furthermore, *MZprox1a*$^{-/-}$,
281 *MZprox1b*$^{-/-}$ mutants initially show a delay in the formation of PLs as these cells emigrate the
282 CV to invest the HM, but despite this delay, these cells eventually seed the HM before failing
283 to undertake any further migration (**Fig 6c; Extended data Fig 5i-m**). We saw evidence for
284 genetic interaction between *prox1a* and *prox1b*, suggesting that both can contribute in
285 zebrafish lymphatic development (**Extended data Fig 5)**.
286
287 To test whether LECs require Prox1a in a cell autonomous manner, we performed embryonic
288 transplantation to generate chimeric embryos, transplanting *MZprox1a*$^{-/-}$ mutant cells into
289 wildtype hosts (**Extended data Fig 6a**). MZ*prox1a*$^{-/-}$ mutant cells failed to form lymphatic
290 vessels in otherwise wildtype hosts and we noted mutant PLs stuck in the HM by 5dpf,
291 confirming that Prox1a functions cell autonomously during zebrafish lymphangiogenesis
292 (**Extended data Fig 6b-d**). Taken together, the *MZprox1a*$^{-/-}$, *MZprox1b*$^{-/-}$ mutant phenotype is
293 more severe than any previously described zebrafish Prox1 mutants and Prox1 is necessary
294 cell autonomously for zebrafish lymphatic development.
295

296 Next, we profiled the endothelium of *MZprox1a*$^{-/-}$, *MZprox1b*$^{-/-}$ mutant zebrafish at 40hpf
297 (when cells are both being specified to LEC fate and sprouting from the CVs) using single cell
298 RNA seq as described above (**Extended data table 5a**). Using cluster analysis and key marker
299 expression, we identified populations of cells that included VECs and also included *prox1a*-
300 positive cells. Based on expression of markers associated with EC sprouting (*mki67*, *pcna*), we
301 defined two populations of secondary sprouts of venous origin (LEC_VEC_01 n=713 cells,
302 LEC_VEC_02 n=677 cells) and a single population of cells representing the cardinal vein (PCV
303 n=812 cells; **Fig 6f-i**). Consistent with our observations in **Fig 1,** cells expressing *prox1a* at
304 40hpf were not transcriptionally distinct from sprouting VECs and failed to form a "lymphatic
305 progenitor" cluster, suggesting they are specified and express *prox1a* but not yet
306 differentiated. RNA velocity analysis suggested that these three clusters remained closely
307 related, consistent with little differentiation between these populations at this stage. To
308 identify the earliest transcriptional changes controlled by Prox1 in lymphatic development,
309 we used DE to evaluate the global differences between *MZprox1a*$^{-/-}$, *MZprox1b*$^{-/-}$ and WT in
310 the LEC_VEC_01 and LEC_VEC_02 clusters of sprouting cells (**Fig 6j, Extended data table 5b**).
311 We found a significant upregulation of a large set of genes in the absence of Prox1 that were
312 identified as enriched for blood vascular and haematopoietic genes by GO-term and marker
313 analysis (**Fig 6k,** n=1,027 genes, **Extended data table 5c**), but we saw little evidence of
314 positively regulated genes downstream of Prox1 (just n=27 genes downregulated in
315 *MZprox1a*$^{-/-}$, *MZprox1b*$^{-/-}$). This demonstrates that in the earliest stages of LEC specification
316 Prox1 is not actively driving a fate program but rather is acting primarily to down-regulate
317 blood vascular and hematopoietic fate. This profile identifies these earliest Prox1-dependent
318 changes.
319
320 **Sprouting Prox1-expressing cells show changes in expression that are not controlled by**
321 **Prox1**
322 During their departure from the CV, zebrafish LECs show differences from sprouting VECs in
323 their proliferation and morphology [40,41]. While Prox1 specifies and maintains LEC fate, these
324 early changes could potentially be regulated by Prox1-independent mechanisms that have
325 yet to be described. To test this, we first examined the 27 genes that we identified as
326 positively regulated in response to Prox1 function (down in mutants; **Fig 6l**). We found that
327 none of these genes were known regulators of lymphangiogenesis. Next, we compared

328 wildtype *prox1a*-expressing and non-expressing cells in the 40hpf secondary sprout clusters
329 using DE analysis (**Fig 6m,o; Extended data table 5d**). We found that n=71 genes were more
330 highly expressed in the early specified Prox1+ LECs than in sprouting VECs, however there was
331 essentially no overlap with the genes that were Prox1-dependent (**Fig 6n**). Despite this, the
332 n=71 genes were clearly enriched for known regulators of early lymphatic vascular
333 development. This included the Yap target *ccn2a,* as well as *s1pr1, nrp2b, rasa1b, mafbb* and
334 *cldn11a*, all up-regulated in LECs at this early stage and previously linked to lymphatic
335 development [42-47] (**Fig 6o**). Together, we take this as evidence that Prox1-independent
336 mechanisms exist in early specified LECs and that they control at least several essential
337 regulators and markers of lymphangiogenesis.
338
339 **Tspan18 homologues are Prox1 targets essential for embryonic lymphangiogenesis**
340 While we find that Prox1 homologues function primarily to negatively regulate gene
341 expression at the earliest stages of lymphangiogenesis, there were still 27 genes positively
342 regulated by Prox1 at 40hpf (**Fig 7a**). One of these genes, *tspan18b* encodes a four-
343 transmembrane domain Tetraspanin protein. Tetraspanins are a highly evolutionarily
344 conserved family of proteins involved in the organisation of membrane microdomains and
345 have been shown to be able to influence cell adhesion, signalling and behaviour [48]. No
346 Tetraspanins have been specifically linked to the process of developmental
347 lymphangiogenesis. We noted that both *tspan18b* and *tspan18a* were down-regulated in
348 *MZprox1a*$^{-/-}$, *MZprox1b*$^{-/-}$ mutants, although *tspan18a* was expressed at much lower levels
349 than *tspan18b* at this stage (**Fig 7a**). In our 4dpf *Zprox1a*$^{-/-}$ mutant dataset, both paralogues
350 were down-regulated in the mutant cluster compared with mature LECs (**Fig 7b**). Both genes
351 displayed expression in LECs in our time course atlas that was enriched in lymphatic vessels
352 compared with muLECs and *tspan18a* was highly enriched in LECs compared with VECs at 3,
353 4 and 5dpf (**Fig 7c**). In our sn-ATAC seq dataset at 4dpf, we identified LEC specific peaks of
354 chromatin accessibility that were increased in the absence of Prox1 for *tspan18b* but Prox1-
355 dependent for *tspan18a* (**Fig 7d**). This suggests that Prox1 regulation of Tspan18 paralogues
356 is likely to be direct in the earliest stages of VEC-LEC transdifferentiation, during specification
357 of the lymphatic lineage. To test if this may be correct and to probe evolutionary conservation
358 of this relationship, we performed ChIP seq for PROX1 in human LECs. We found that PROX1
359 binds directly to intragenic sites and the TSS at the *TSPAN18* locus in human LECs (**Fig 7e**).

360

361 Finally, we tested if *tspan18a* and *tspan18b* are functionally relevant targets of Prox1 in
362 zebrafish lymphatic development. We used a CRISPR F0 knockout approach[49] and confirmed
363 CRISPR targeting by PCR. We carefully quantified LEC numbers in the trunk of
364 *tspan18a/tspan18b* crispants at 5dpf and found a loss of lymphatic vessels and strong
365 reduction in LEC numbers but no change in the number of VECs in venous ISVs, which form
366 concomitant with LECs during secondary sprouting (**Fig 7f**). The reduction in LECs in this
367 setting was not a phenocopy of the more severe phenotype in *MZprox1a*$^{-/-}$, *MZprox1b*$^{-/-}$
368 mutants, suggesting that the *tspan18* paralogues likely perform only a part of the job
369 necessary for normal lymphatic development downstream of Prox1 (**Fig 7f**). Overall, the
370 example of *tspan18a* and *tspan18b* demonstrates the utility of this resource of singe cell RNA
371 and snATAC seq data for the discovery of highly conserved targets of Prox1 and of functionally
372 relevant regulators of lymphatic development.

373

374 **Discussion**

375 In this study, we present a single cell RNA seq analysis of four key stages of embryonic
376 lymphangiogenesis in a vertebrate embryo, revealing new markers and potential regulators
377 of LEC differentiation. We profile the endothelial cells of *Zprox1a* mutants, which form
378 lymphatic structures, but these "lymphatics" dedifferentiate. This identifies the
379 transcriptional code maintained by Prox1 in order to maintain LEC identity and the highly
380 conserved nature of Prox1 function comparing zebrafish with mice. We further probed the
381 *Zprox1a* mutant model using snATAC seq and found that while in mutants the transcriptome
382 reverts to a blood vascular fate in the absence of Prox1, the chromatin displays ectopically
383 open regions and peaks that suggest a more immature state. In particular, in the absence of
384 Prox1 at 4dpf, a large number of opened chromatin regions are enriched for transcription
385 factor motifs for earlier acting vasculogenic and haematopoietic transcription factors. This
386 suggests that regulators of earlier vascular fate become more active and increase chromatin
387 accessibility in the absence of Prox1. This role of Prox1 has not been previously appreciated
388 and this may suggest its combinatorial function with other developmental transcription
389 factors that are dysfunctional in the absence of Prox1.

390

391 Additional biological insights from this study come from our analysis of double maternal
392 zygotic *prox1a, prox1b* mutants. These mutants are presumed "null" mutants for Prox1
393 orthologues and they revealed (through scRNA seq) that during its earliest role in vascular
394 development, in LEC fate specification and VEC-LEC transdifferentiation, Prox1 functions
395 primarily to negatively regulate blood and blood vascular fate. While this may represent a
396 downstream program rather than direct repression of gene expression by Prox1 orthologues,
397 it is notable that Prox1 and *Drosophila* Prospero have been reported to be able to function as
398 repressors in a context dependent manner [50-54]. We also found that there is significant change
399 in early sprouting *prox1a*-positive LECs that is not regulated by Prox1-function. While this may
400 seem counter-intuitive, many of the genes increased in these cells independent of Prox1
401 function are already implicated in lymphatic development and we take this to suggest that
402 mechanisms regulated independently of Prox1 homologues exist in the earliest sprouting
403 LECs. The regulators of these factors at this stage remain to be described. Finally, by further
404 characterisation of Prox1 regulation of Tspan18 homologues (a and b), we identify that Prox1
405 controls lymphangiogenesis through a previously undescribed factor that is likely to act at the
406 LEC membrane. The Tspan18 CRISPR knockout phenotype is more subtle than *MZprox1a*$^{-/-}$,
407 *MZprox1b*$^{-/-}$ mutants, suggesting that multiple downstream targets are likely at play and
408 orchestrate lymphatic development in response to Prox1 function.
409
410 Altogether this study describes the process of developmental venous to lymphatic
411 transdifferentiation, early LEC differentiation and LEC maintenance in detail, *in vivo*. We
412 describe the role of Prox1 during this process, revealing a conserved and dynamic regulatory
413 process with unprecedented resolution. This resource will help to understand
414 lymphangiogenesis in contexts beyond the embryo, such as in pathological
415 lymphangiogenesis in metastasis, inflammation and tissue repair. Finally, we suggest that
416 combining zebrafish mutant models, with their inherent ease of cellular accessibility, and the
417 resolution afforded by single cell profiling, will be an approach that yields powerful new
418 insights in many areas of developmental biology in the future.
419
420 **Acknowledgements**
421 This project was supported in part by NHMRC Ideas grant 2004300 and ARC Discovery project
422 DP180102846. B.M.H. was supported by NHMRC Fellowship 1155221. We thank Angelika

Christ and the IMB Sequence Facility (University of Queensland), Tim Semple and Peter Mac Genomics Facility, the Research Computing Facility at Peter Mac, FACS facilities at UQ and Petermac and Isaac Virshup for assistance.

Author contributions

L.G. and E.M. performed, analysed experiments and co-wrote manuscript. B.M.H, K.K and N.L.H conceptualised experiments, analysed data and co-wrote manuscript. S.D, T.C, O.Y, N.I.B, S.P, K.O, A.S and A.L. performed and analysed experiments. J.P, and K.A.S, provided key unpublished reagents and analysed data.

Conflicts of interest

The authors declare no conflict of interests.

Online Methods

Zebrafish husbandry

Zebrafish work was conducted in compliance with animal ethics committees at the Peter MacCallum Cancer Centre, the University of Melbourne and the University of Queensland. Published transgenic lines used were: *Tg(fli1a:nEGFP)*^{y7} [55]*; Tg(-5.2lyve1b:DsRed)*^{nz101} [24]*;* and *Tg(kdrl:Has.HRAS-mCherry)*^{s916} [21]*.* Published mutant lines used were *prox1a*^{i278} [20], *prox1b* [4,19]. *Tg(lyve1b:Venus)*^{uq51bh} was generated as previously described[28] but here using an independent genomic integration with the same construct.

Generation of maternal zygotic mutants

Germline replacement was performed using embryonic transplantation as previously described [4,56]. Maternal zygotic (MZ) *prox1a* mutant embryos were made by crossing germline replaced *prox1a*$^{i278-/-}$;*prox1b*$^{sa0035+/-}$ females with *prox1a*$^{i278+/-}$;*prox1b*$^{sa0035+/-}$ males [4,56]. Genotyping of individual embryos during transplantation and phenotypic analysis was performed as previously described [4].

Transgenesis, genome-editing and genotyping

All microinjections were performed as previously described [57]. CRISPR genome editing for *tspan18a/b* was performed as previously described [58], and all genotyping confirmed using

455 PCR [49]. *slc7a7a*^{BAC}*:slc7a7a-Citrine*^{uom10} and *fabp11a*^{BAC}*:fabp11a-Citrine*^{uom10} recombineering
456 was performed as previously described [59].
457 Guide RNA primers previously described [49]:
458 *tspan18a*-T1-5'-CCCAGATTCCCACCCCTAGA-3' (product size 290bp)
459 *tspan18a*-T2-5'-GGCGGGATGCTGTTCCTACT-3' (product size 270bp)
460 *tspan18b*-T1-5'-TGAAGCCTCCCCGAGCCCCT-3' (product size 285bp)
461 *tspan18b*-T2-5'-TGTGGACCCCACAGGATTTA-3' (product size 110bp)
462 Primers for PCR genotyping:
463 *tspan18a*-T1-geno-forward:5'-AGTGCTGTGGGAAAATGAGC-3'
464 *tspan18a*-T1-geno-reverse:5'-AAATCCCATACAAACAATAGAAGG-3'
465 *tspan18a*-T2-geno-forward:5'-AGTGCTGTGGGAAAATGAGC-3'
466 *tspan18a*-T2-geno-reverse:5'-AAATCCCATACAAACAATAGAAGG-3'
467 *tspan18b*-T1-geno-forward:5'-AGTGCTTTAGTATGCATGTTTCTGT-3'
468 *tspan18b*-T1-geno-reverse:5'-TGCTAGATCAATCGTGGAATGG-3'
469 *tspan18b*-T2-geno-forward:5'-GTGGCTCGTTCCTCCTCG-3'
470 *tspan18b*-T2-geno-reverse:5'-CAGGATGATGTAGACGCCCG-3'
471 Primers for BAC recombineering:
472 *slc7a7a*-BAC-Citrine-forward:5'-
473 AACTGCTTTAGACAGTGTTTTTTGGTACCATCCCATATATTTAAAAAACAGCCACCATGGTGA
474 GCAAGGGCGAGGAG-3'
475 *slc7a7a*-BAC-Citrine-reverse:5'-
476 TTCGACACCTCAGGGGATGCCTCTTCTGCAGGCGTAGGGCTGTAGGACGCTCAGAAGAACT
477 CGTCAAGAAGGCG-3'
478 *fabp11a*-BAC-Citrine-forward:5'-
479 TTACAGCTGTTGCGAGATTGAAAAGTAGAGGAGCATCATTATTCGGGAAAGCCACCATGGT
480 GAGCAAGGGCGAGGAG-3'
481 *fabp11a*-BAC-Citrine-reverse:5'-
482 TCAAAGTTGTCGCTGGTGGTCATTTTCCACGTTCCTACGAATTTGTCAACTCAGAAGAACTC
483 GTCAAGAAGGCG-3'
484
485 **Imaging and quantification**
486 Imaging was conducted at the Centre for Advanced Histology and Microscopy (Peter

487 MacCallum Cancer Centre). Imaging of live samples was performed using a Zeiss LSM 710 FCS
488 confocal microscope, a Zeiss LSM 780 FCS confocal microscope, or an Olympus FV3000
489 confocal microscope. Mounting and imaging were performed as previously described [60].
490
491 In Figs. 2b, 6a-c, and 7f, quantification of vascular phenotypes was performed as previously
492 described [60,61]. In Figs 3h-k, *cdh5:Venus* or *kdrl:GFP* intensity in the TD was measured using
493 Imaris software (Bitplane) and normalised to fluorescence intensity of the DA for *cdh5* and to
494 the fluorescence intensity PCV for *kdrl* in the same embryos.
495
496 **Fluorescence activated cell sorting**
497 FACS was performed at the Peter MacCallum Cancer Centre and the University of
498 Queensland. For **Fig 1**, we isolated cells using the following transgenic lines: 40hpf,
499 *Tg(fli1a:nEGFP)*^{y7}; 3,4 and 5dpf, *Tg(-5.2lyve1b:Venus)*^{uq47bh}, *Tg(kdrl:Has.HRAS-mCherry)*^{s916}
500 For **Fig 3 and Fig 4**, we isolated cells using the following transgenic lines: 4dpf,
501 *Tg(fli1a:nEGFP)*^{y7}, *Tg(-5.2lyve1b:DsRed)*^{nz101}. For **Fig 6**, we isolated cells using the following
502 transgenic lines: 40hpf, *Tg(fli1a:nEGFP)*^{y7} .To dissociate embryos and obtain single cell
503 suspensions, we followed published protocols [62]. Briefly, at the desired developmental stage
504 we deyolked embryos by pipetting up and down and rinsing in calcium free ringers solution,
505 we centrifuged at 2000rpm for 5' at 4°C and remove supernatant and dissociated the cells by
506 incubating in liberase [2.5mg/mL] (Cat #5401119001 Sigma-Aldrich) diluted at a 1:35 ratio in
507 DPBS at 28.5°C for approximately 5', homogenizing the samples during and after the
508 incubation. To stop the reaction, we added CaCl2 to a final concentration of 1-2mM and FBS
509 to a final concentration of 5-10%. We centrifuged at 2000rpm for 5' at 4°C. discarded the
510 supernatant, in order to be able to asses live vs. dead cells, we re-suspend the cells solution
511 in Zombie Violet TM Viability Dye (Cat# 423113, BioLegend) and incubated for 20' at RT softly
512 rocking, we rinsed the cells by centrifuging and resuspending in DPBS/EDTA, for ATAC-seq
513 experiments samples were resuspended in 2%BSA/PBS. Suspension was filtered through a
514 strainer and taken to the FAC sorting facility. In the Flow Cytometry facility, we used the BD
515 FACS Aria Fusion sorter (BD Biosciences), we based the selection for the desired population
516 on FSC and SCC, alive cells were selected based on the Zombie Violet profile and double
517 positive cells for the desired transgenics were targeted according to the expression profiles

518 of single cells. Double positive cells were sorted in 300uL 100% FBS in a cold block and taken
519 immediately to the sequencing facility.
520
521 **scRNA-seq library preparation**
522 Library preparation and sequencing was performed at the Institute for Molecular Bioscience
523 Sequencing Facility (University of Queensland) or Peter Mac Genomics Facility. Single cell
524 suspensions were sorted by FACS, spun down to concentrate and a cell count was performed
525 to determine post-sort viability and cell concentration. Single cell suspension was partitioned
526 and barcoded using the 10X Genomics Chromium Controller (10X Genomics) and the Single
527 Cell 3' Library and Gel Bead Kit (V2 10X Genomics PN-120237; V3.1; 10X Genomics; PN-
528 1000123). The cells were loaded onto the Chromium Single Cell Chip A (10X Genomics; PN-
529 120236), B (10X Genomics; PN-1000073 or PN-1000074) or G (10X Genomics; PN-1000120)
530 to target 10,000 cells. GEM generation and barcoding, cDNA amplification, and library
531 construction was performed according to the 10X Genomics Chromium User Guide. The
532 resulting single cell transcriptome libraries contained unique sample indices for each sample.
533 The libraries were quantified on the Agilent BioAnalyzer 2100 using the High Sensitivity DNA
534 Kit (Agilent, 5067-4626). Libraries were pooled in equimolar ratios, and the pool was
535 quantified by qPCR using the KAPA Library Quantification Kit - Illumina/Universal (KAPA
536 Biosystems, KK4824) in combination with the Life Technologies Viia 7 real time PCR
537 instrument. After the initial sequencing run, libraries were re-pooled according to estimated
538 captured cells as determined using the Cell Ranger software (10X Genomics).
539
540 **Sequencing of scRNA-seq libraries**
541 At the IMB(UQ) genomics facility, denatured libraries were loaded onto an Illumina NextSeq-
542 500 and sequenced using a 150-cycle High-Output Kit as follows: 26bp (Read1), 8bp (i7 index),
543 98bp (Read2). Read1 supplies the cell barcode and UMI, i7 the sample index, and Read2 the
544 3' sequence of the transcript. At the Peter Mac Molecular Genomics facility, single cell
545 transcriptome libraries were sequenced on an Illumina NovaSeq 6000 using S4 300-cycle
546 chemistry. Read1 supplies the cell barcode and UMI, i7 the sample index, and Read2 the 3'
547 sequence of the transcript. Sequencing read lengths were trimmed to 28bp (Read1), 8bp (i7
548 index), 91bp (Read2), ensuring compatibility with the 10X Genomics analysis software, Cell
549 Ranger.

550

551 **scRNA-seq data processing and analysis**

552 All code and documentation associated with this analysis is publicly available under an open
553 source software license at:
554 https://atlassian.petermac.org.au/bitbucket/users/tyrone.chen/repos/hogan_lab/browse/2
555 022_Grimm_Mason_et_al_PROX1/
556 Relevant functions are in italics for reference. Where necessary fastq files were made using
557 *Cell Ranger* [63] (version 3.1.0 or 3.0.2) *mkfastq*. Sequencing QC was assessed using *FastQC*
558 0.11.6 and *MultiQC* viewer for aggregated reports. *Cell Ranger count* and *aggr* were used to
559 generate aggregated count files mapped to GRCz11 (Ensembl 101), without depth
560 normalisation. Doublets were identified from the filtered aggregated count files using
561 *Scrublet* [64] in *Python* version 3.6 and filtered from subsequent analyses. For the *MZprox1*$^{-/-}$
562 mutant and *Zprox1*$^{-/-}$ mutant datasets filtered aggregated count files were processed, sc-
563 transform normalised, filtered and clustered (louvain) using *Seurat* version 2.0 [65] and 3.0 [34]
564 respectively for *R statistical software* version 4.0.2. QC was evaluated before and after
565 normalisation using plot functions in *Seurat* and *scater* 1.20.1 [66], and all thresholds and
566 settings are described in scripting. Cluster solutions were evaluated using *ClusTree* [67].
567 Datasets used in the atlas of lymphangiogenesis were processed, filtered, merged and log-
568 normalised using *Seurat* version 3.0 [34], with QC and settings as above. Merged data was
569 clustered and normalised using *CSS simspec* [33] and clustering and cluster evaluation
570 performed on this object only, as described above. For all scRNA-seq datasets cluster
571 phenotype was determined using the expression of key markers (Supplementary Table), with
572 the aid of *CellXGene* visualisation software [68]. All downstream analysis and plotting were
573 performed using *Seurat* version 3.0 [34] with default settings. All gene ontology analyses were
574 performed using Panther.db [37] (Biological Process Complete).

575

576 **Preparation of single nuclei for snATAC-seq**

577 Single cell suspensions were sorted by FACS and prepared for nuclei isolation as previously
578 described by 10x Genomics Demonstrated Protocol for Single Cell ATAC Sequencing
579 (CG000169 - Rev D). Cell suspensions were pelleted (300 x g for 5 minutes) and rinsed with
580 PBS + 0.04% BSA. Cells were resuspended in 95uL of freshly prepared lysis buffer (10mM Tris-
581 HCl pH 7.4, 10 mM NaCl, 3 mM MgCl2, 0.1% Tween-20, 0.1% NP40 Substitute, 0.01%

582 Digitonin, and 1% BSA) and incubated on ice for 1 minute. 100uL of chilled wash buffer
583 (10 mM Tris-HCl, pH 7.4, 10 mM NaCl, 3 mM MgCl2, 0.1% Tween-20, 1% BSA) was used to
584 neutralise the reaction, before the nuclei were pelleted (500 x g for 5 minutes) and
585 resuspended again in 7uL of 1x Nuclei Buffer (10X Genomics Cat# PN-2000153/2000207).
586 Presence of healthy and intact nuclei was assessed by visual inspection on a brightfield
587 microscope using Trypan Blue staining (Thermo Fisher Cat# T10282) and Countess Cell
588 Counting Chamber Slides (Thermo Fisher Cat# C10228).
589
590 **snATAC-seq library preparation and sequencing**
591 Single nuclei suspensions were resuspended at approximately 5000 nuclei per μL before
592 undergoing tagmentation for 60min at 37°C. After tagmentation nuclei were partitioned and
593 barcoded using the 10X Genomics Chromium Controller (10X Genomics) and the Single Cell
594 ATAC Reagent Kit (V1.1; 10X Genomics; PN-1000176). Tagmented nuclei were loaded onto
595 the Chromium Single Cell Chip H (10X Genomics; PN-1000162), GEM generation, barcoding
596 and library construction was performed according to the 10X Genomics Chromium User
597 Guide. The resulting single cell ATAC libraries contained unique sample indices for each
598 sample. The libraries were quantified on the Agilent BioAnalyzer 2100 using the High
599 Sensitivity DNA Kit (Agilent, 5067-4626) and pooled in equimolar ratios. Sequencing was
600 performed on an Illumina NextSeq 500 using a 150-cycle High-Output Kit as follows: 50bp
601 (Read1), 8bp (i7 index), 16bp (i5 index), 50bp (Read2) achieving a read depth of 25,000 read
602 pairs per nucleus.
603
604 **snATAC-seq processing and analysis**
605 FASTQ files generated from sequencing were used as inputs to 10X Genomics *Cell Ranger*
606 *ATAC 2.0.0*. *cellranger-atac count* was used to generate count files mapped to GRCz11
607 (ENSEMBL 101), without depth normalisation. Resulting fragment files were read into *ArchR*
608 *1.0.1* for *R statistical software 4.0.5* as a tile matrix with 500-bp bins. All remaining steps in
609 the ATAC-Seq analysis were performed within *ArchR 1.0.1*. QC filtering was performed, and
610 only high-quality cells with a TSS enrichment score greater than 4 and greater than 1,000
611 unique nuclear fragments were retained. Doublets were predicted using *addDoubletScores*
612 and filtered using *filterDoublets.* Data normalization and dimensionality reduction were
613 performed using iterative Latent Semantic Indexing (LSI) and Uniform Manifold

614 Approximation and Projection (UMAP) embeddings were used for visualisation in reduced
615 dimension space. Separate from the *ArchR 1.0.1* package, cluster solutions were
616 independently evaluated using *clustree 0.4.3*. A Gene Score Matrix that stores predicted gene
617 expression was then generated based on the accessibility of regulatory elements in the
618 vicinity of the gene. We used gene scores of endothelial markers for cluster annotation and
619 subsetting. Differentially accessible genes were identified by differential testing using
620 *getMarkerFeatures*. Local chromatin accessibility of the marker genes was visualised using
621 the *plotBrowserTrack*.
622
623 **ChIP-seq library preparation and analysis**
624 For ChIP, antibodies used were goat anti-Prox1 (R&D Systems, AF2727), rabbit anti-H3K4Me1
625 (Cell Signaling, #5326), rabbit anti-H3K27Me3 (Cell Signaling, #9733), rabbit anti-H3K27Ac
626 (Cell Signaling, #8173), rabbit anti-H3K4Me3 (Cell Signaling, #9751). hLEC were harvested and
627 processed for ChIP as previously described[69] using a truChIP™ Low Cell Chromatin Shearing
628 Kit with SDS Shearing Buffer (Covaris). Briefly, 10 million cells/ml were cross-linked using 1%
629 formaldehyde for 5 minutes, neutralised with glycine, lysed and nuclei washed. For
630 transcription factor ChIP, chromatin from 3 million cells was sheared using a 130µl microtube
631 in a Covaris sonicator at the recommended settings for 8 minutes. 5µg antibody was used to
632 immunoprecipitate sheared DNA. For histone mark ChIP, chromatin from 1 million cells was
633 sheared and 1µg antibody was used. Following washing and reversal of crosslinks, DNA was
634 purified using a Qiagen MinElute PCR Purification Kit. ChIP-Seq library preparation and
635 sequencing was carried out at the ACRF Cancer Genomics Facility, Centre for Cancer Biology,
636 Adelaide. ChIP-Seq libraries were prepared according to Illumina's TruSeq Sample Prep Guide
637 Revision A with some minor modifications as previously described[69]. Briefly, DNA was end-
638 repaired, followed by adenylation of the 3' ends. Next, Illumina indexing adapters were
639 ligated to the DNA. 18 cycles of PCR were performed to enrich for successfully adapter ligated
640 molecules. Ligation products were purified with a 2% Pippin Prep gel (Sage Science), selecting
641 a size range of 250 – 300 base pairs. The size distribution and yield of the purified libraries
642 were determined using an Agilent Bioanalyzer High Sensitivity chip and Qubit dsDNA HS assay
643 (Invitrogen), respectively. Libraries were pooled in equimolar ratios and sequenced in one
644 lane of a HiSeq 2500 short read flowcell (1 x 50bp). Reads were mapped to the UCSC hg19
645 genome with BWA[70] version 0.7.9a-r786, allowing at most 3 alignments. Read depth was

646 calculated via *genomeCoverageBed* from BEDTools[71], using the scale parameter to normalise
647 to reads-per-million. Read depth was plotted relative to annotated transcription start sites
648 via custom Python scripts utilising Matplotlib.
649
650
651

652 **FIGURES AND FIGURE LEGENDS**

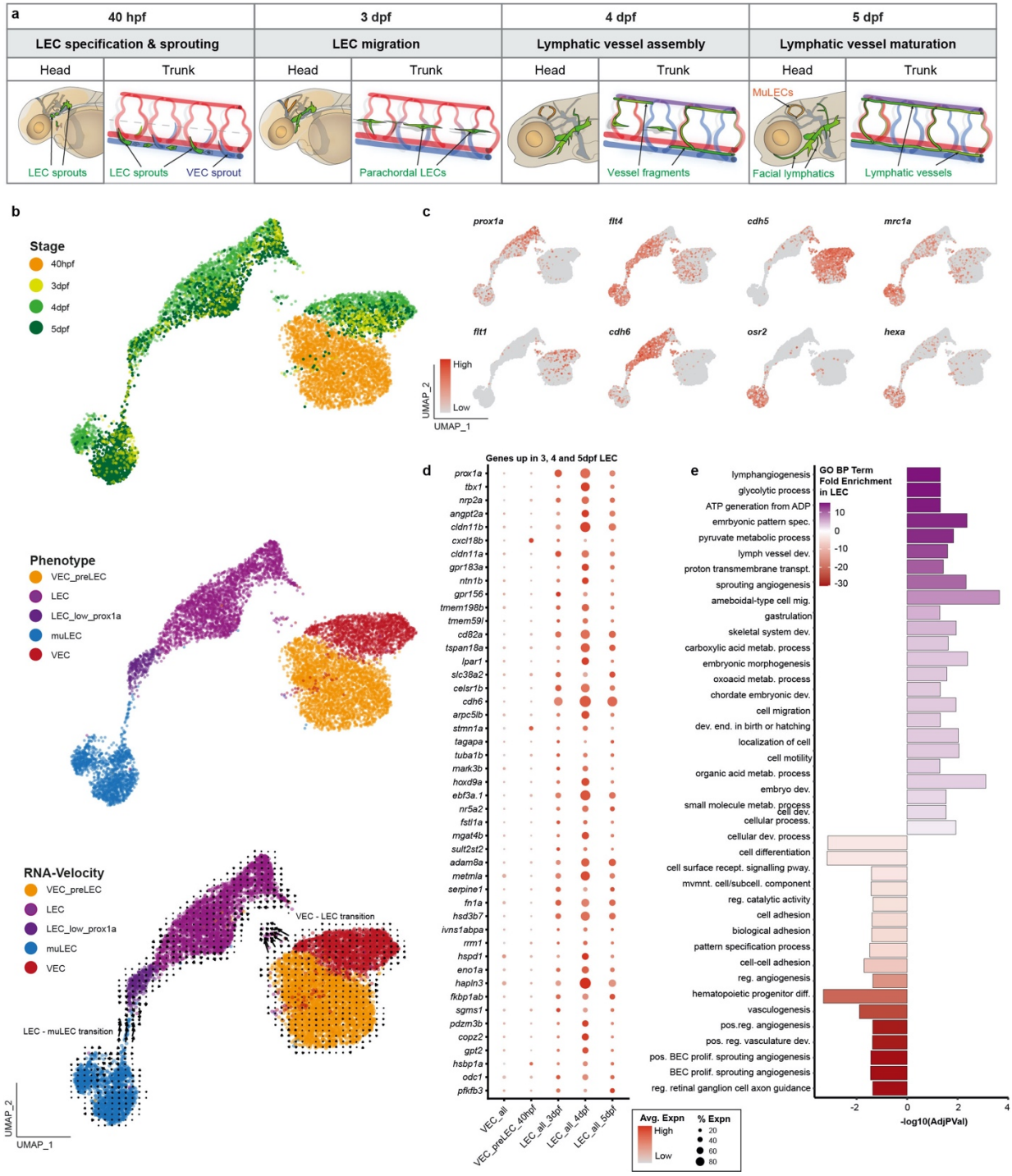

653

654 **Figure 1: A single cell RNAseq developmental atlas of lymphangiogenesis in zebrafish**

655 **a.** Schematic representation of four key stages of zebrafish lymphatic development in
656 head and trunk: 40hpf encompasses both specification (Prox1-induction) and
657 sprouting; 3dpf migration of LECs; 4dpf assembly of lymphatic vessels; 5dpf
658 maturation functional lymphatics.

659 **b.** UMAP visualization of 9771 cells filtered for VEC and LEC populations (n=6 samples;
660 see **Extended data table 1a** for cluster identification and **Extended data fig 1** for whole
661 dataset) coloured according to developmental stage (top), predicted cell phenotype
662 (middle), and RNA-velocity (bottom).
663 **c.** UMAP visualization of key marker gene expression. Colour scale represents log-
664 normalised expression. LEC markers: *prox1a, cdh6*. BEC marker: *cdh5*. LEC and VEC
665 markers: *mrc1a, flt4*. AEC marker: *flt1*. muLEC markers: *osr2, hexa*.
666 **d.** Dot plot of top genes commonly marking LECs at 3, 4 and 5dpf, with expression
667 displayed in VECs (all stages), VEC_preLEC (40hpf) and LECs at 3, 4 and 5dpf (see also
668 **Extended data table 1b**, **Extended data figure 1f**). Colour scale represents average
669 log-normalised expression and point size represents percentage of cells expressing
670 gene.
671 **e.** Bar plot summarizing GO BP analyses of genes DE between 3, 4 and 5dpf LEC and VEC
672 populations (**Extended data table 1c-d**). Y-axis represents enriched BP term, x-axis
673 represents the -log10(*adjusted p value*), bars are coloured and ordered according to
674 fold enrichment of the GO term in LEC. GO terms enriched in LEC are coloured purple,
675 terms enriched in VEC are coloured red.
676 Hpf, Hours post-fertilisation.dpf, Days post fertilisation. BEC, Blood vascular endothelial cell.
677 VEC, Venous endothelial cell. LEC, Lymphatic endothelial cell. muLEC, mural Lymphatic
678 endothelial cell (a.k.a FGP or brain LEC).
679
680
681

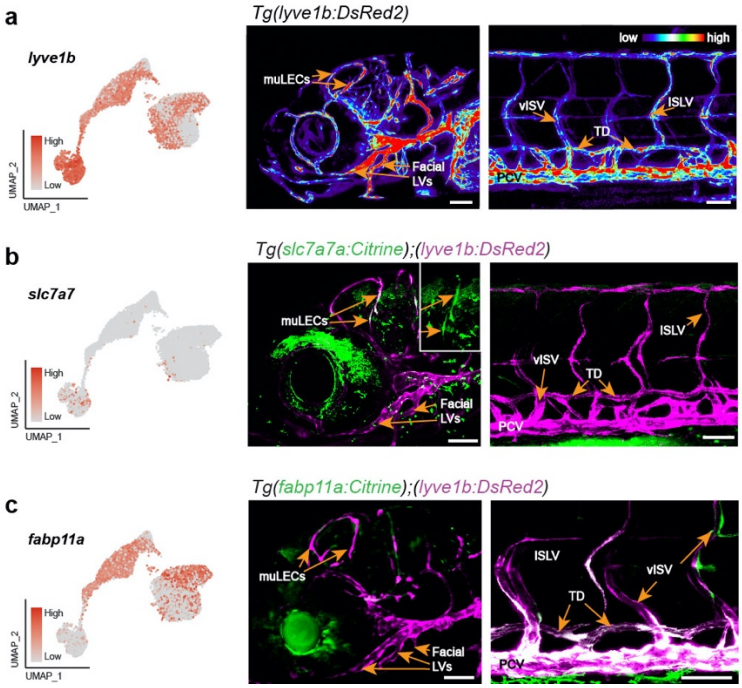

Figure 2: Transgenic marker strains confirm cluster identity and identify vessel specific markers

- **a.** UMAP of *lyve1b* expression predicts higher expression in muLECs than LEC populations (left), confirmed by a heat map of a *Tg(lyve1b:DsRed2)* zebrafish larvae at 6dpf showing high *lyve1b* expression in craniofacial (middle) and moderate expression in trunk lymphatic vessels (right).
- **b.** UMAP of *slc7a7a* expression predicts restricted expression in muLEC populations (left), confirmed in lateral confocal projections showing co-expression of *lyve1b* (magenta) and a new BAC transgenic strain for *slc7a7* (green) in the zebrafish head at 5dpf (middle) which is not expressed in veins and lymphatic vessels of the trunk (right).
- **c.** UMAP of *fabp11a* expression predicts expression in LEC and VEC but not muLEC populations (left), confirmed in lateral confocal projections showing co-expression of *lyve1b* and a new BAC transgenic strain for *fabp11a* marking venous and lymphatic vessels in the trunk (right) without showing expression in the vasculature of the head (middle) at 5dpf.

Lateral confocal images, anterior to the left. muLECs, mural lymphatic endothelial cells; facial LV, facial lymphatic vessels; vISV, venous intersegmental vessel; PCV, posterior cardinal vein; TD, thoracic duct; ISLV, intersomitic lymphatic vessel. Scale bars, 80 µm for head (middle) in (a) and 50 µm for trunk images (right).

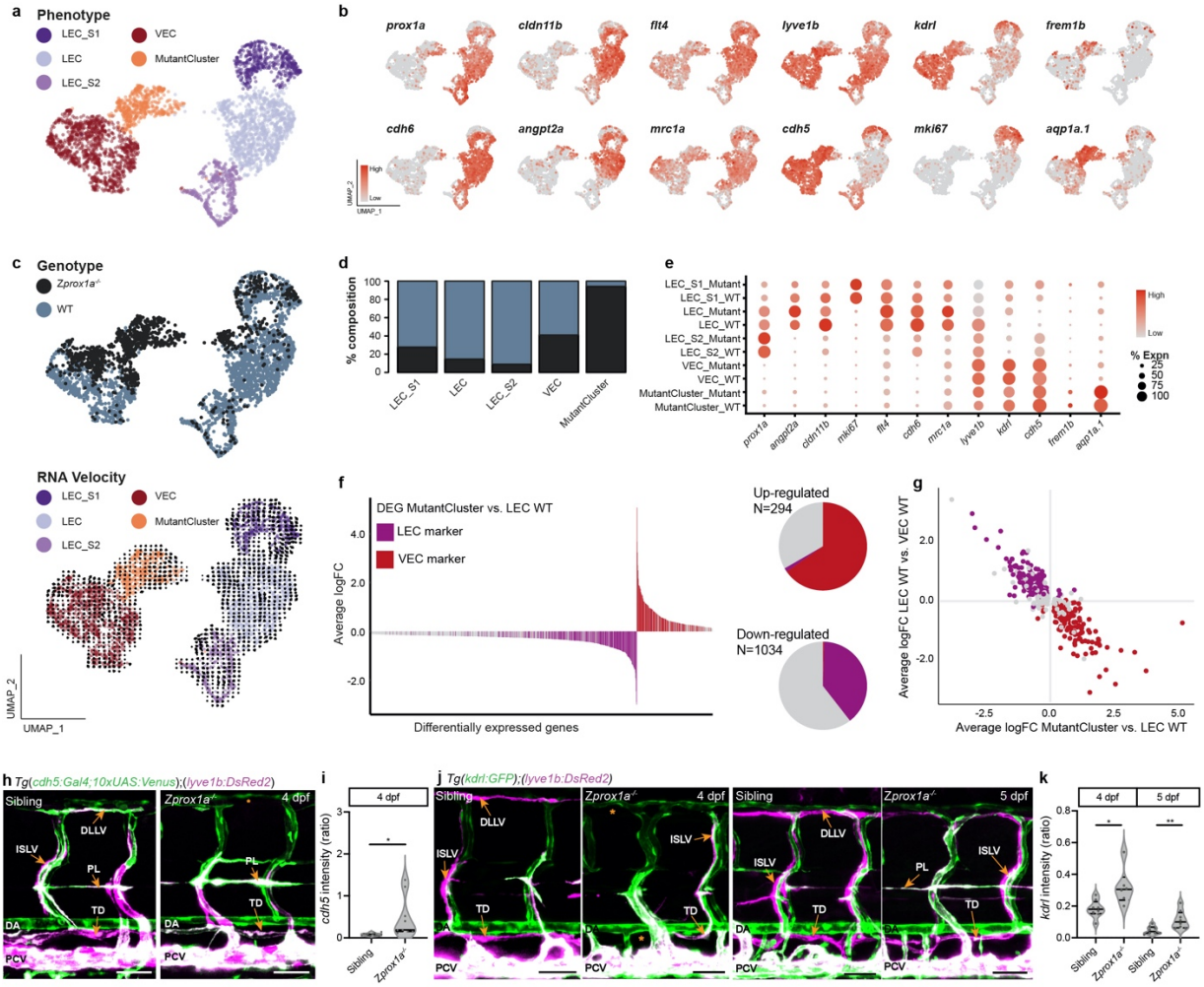

Figure 3: Single cell RNA seq analysis reveals a fate shift from LEC to VEC in the absence of Prox1 in zygotic *prox1a* mutants

a. UMAP visualization of 8075 cells filtered for VEC and LEC subpopulations (n=2 samples; see **Extended data table 2a** for cluster annotation, **Extended data Fig3** for full dataset) coloured according to predicted cell phenotype.

b. UMAP visualization of marker gene expression. Colour scale represents SCT-normalised expression. LEC markers: *prox1a, cldn11b, cdh6, angpt2a*. LEC and VEC markers: *flt4, mrc1a, lyve1b*. BEC markers: *cdh5, kdrl*. Mutant cluster markers: *frem1b, aqp1a.1.*

c. UMAP visualization with cells coloured according to genotype (*Zprox1a*$^{-/-}$ or WT) identifies a mutant specific cluster and RNA velocity analysis suggests a trajectory between the mutant cluster and the LEC cluster, likely indicative of a fate shift.

d. Stacked bar plot representing the genotype composition of cells in a given phenotypic cluster.

717 **e.** Dot plot of marker expression across defined clusters (indicated on Y-axis). Colour
718 scale represents average SCT-normalised expression and point size represents
719 percentage of cells expressing gene.
720 **f.** Bar plot of average log fold change in gene expression comparing WT LECs with the
721 Mutant Cluster. Y-axis represents average log fold change, x-axis represents
722 differentially expressed genes (Wilcoxin Rank Sum *adjusted p value* < 0.05) and bars
723 are coloured according to status as a LEC (purple) or VEC (red) marker in **Fig. 1**. Pie
724 charts (right) indicate the LEC and VEC marker composition of genes up-regulated
725 (n=365) and down regulated (n=1922) in the Mutant Cluster, demonstrating a fate
726 shift.
727 **g.** Concordance in the fate shift between Mutant Cluster and WT LEC with the WT LEC
728 and VEC trajectory. Each point represents significant DE genes (n=2287) between
729 Mutant Cluster and LEC WT, coloured according to LEC or VEC marker status. X-axis
730 represents average log fold change relative to the Mutant Cluster, Y-axis represents
731 average log fold change relative to LEC WT.
732 **h.** Lateral confocal images of *cdh5* (green) and *lyve1b* (magenta) expression in the
733 developing trunk in WT and *Zprox1a* mutants at 4dpf.
734 **i.** Quantification of *cdh5* intensity in the thoracic duct in WT and mutants (relative to
735 expression in the DA).
736 **j.** Lateral confocal images of *kdrl* (green) and *lyve1b* (magenta) expression at 4dpf (left)
737 and 5dpf (right).
738 **k.** Quantification of *kdrl* intensity in the thoracic duct in WT and mutants (relative to
739 expression in the PCV) at 4 and 5dpf.
740 WT, wildtype. Z, zygotic. TD, thoracic duct, DA, Dorsal Aorta. PCV posterior cardinal vein. ISLV,
741 intersomitic lymphatic vessel. DLLV, Dorsal longitudinal lymphatic vessel. PL, parachordal LEC.
742 Scale bars, 50 µm. *, The error bars represent mean ± s.e.m.; *p=0.01 and **p=0.0094 from
743 an unpaired, two-sided t-test.
744

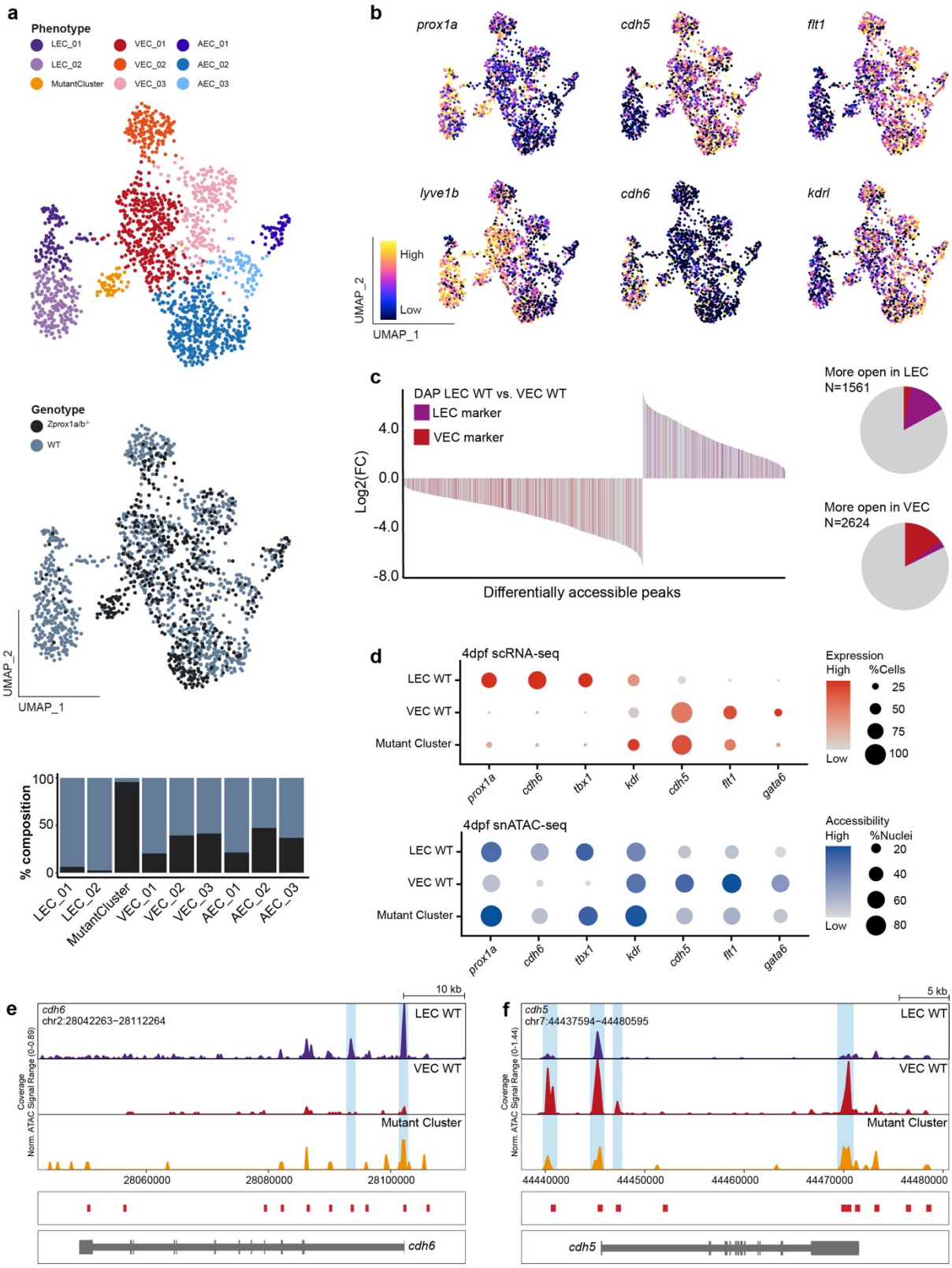

Figure 4: Single nuclei ATAC seq reveals chromatin accessibility changes between venous and lymphatic endothelial cells

a. UMAP visualization of snATAC-seq from *Zprox1a*$^{-/-}$ mutant and WT endothelial cells at 4dpf (n=3731 nuclei), coloured by cell phenotype (top) and genotype (middle) (see

750 **Extended data Fig4** for full dataset). Bar plot summarising the composition of wildtype
751 and mutants in each cluster. A mutant specific cluster is identified, similar to **Fig 3**.
752 **b.** UMAPs visualization indicating accessibility of key marker genes (gene score) that
753 confirm predicted cluster phenotypes.
754 **c.** Bar plot of log2 fold change for the differentially accessible peaks (n=4185 peaks,
755 Wilcoxon Rank Sum, *FDR* < 0.05) between WT LECs and WT VECs. LEC/VEC markers
756 identified in scRNA-seq are coloured in red/purple respectively and demonstrate a
757 strong correlation between chromatin state and the VEC to LEC fate shift. 228/1561
758 more accessible peaks in the LEC cluster were associated with LEC markers and
759 398/2624 more accessible peaks in VEC cluster associated with VEC markers. Pie
760 charts (right) summarising the proportion of LEC/VEC markers in the differentially
761 accessible peaks.
762 **d.** Dot plots of scRNA-seq (top) and snATAC-seq accessibility (bottom) data summarising
763 the behaviour of key LEC (*prox1a, cdh6, tbx1*) and VEC (*cdh5, flt1, gata6*) markers in
764 WT LECs, WT VECs and the Mutant Cluster at 4dpf. LEC genes are upregulated (scRNA-
765 seq) and chromatin is more permissive (snATAC-seq) in WT LEC, and VEC genes are
766 upregulated and more permissive in WT VEC. The size of the dots represents the
767 proportion of cells or nuclei, and colour represents either SCT-normalised expression
768 or Gene Score of Accessibility.
769 **e.** Genome accessibility track of LEC marker *cdh6* (left) and VEC marker *cdh5* (right)
770 indicating these genes are more accessible in WT LEC and WT VEC cell phenotypes
771 respectively. Red bars represent peaks in the reproducible peak set from snATAC-seq.
772 DAP between WT LECs and WT VECs (Wilcoxon Rank Sum, *FDR* < 0.05) were
773 highlighted in blue.
774
775 DAP, differentially accessible peaks. FDR, false discovery rate. snATAC-seq, single nuclei
776 ATAC-seq.
777

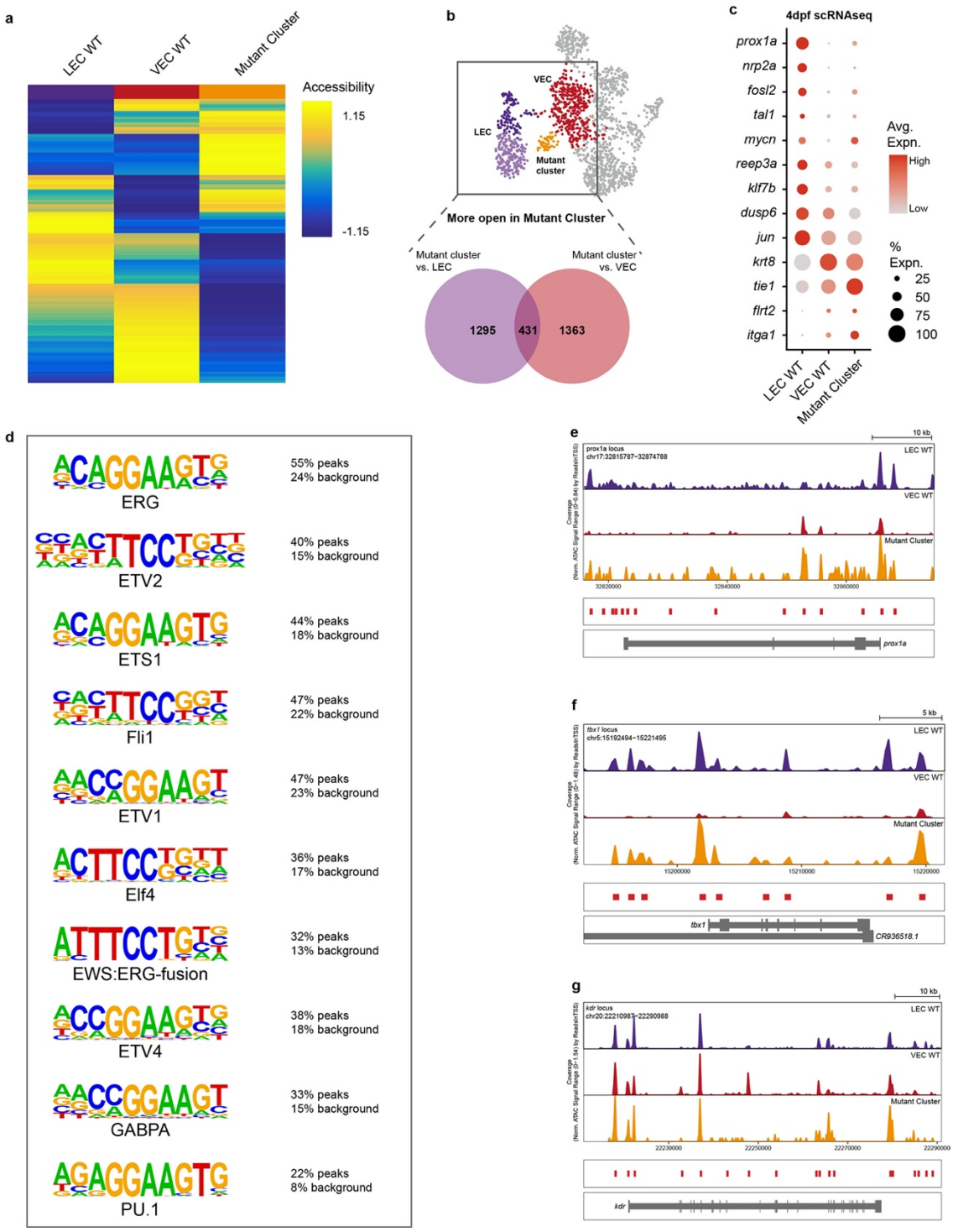

Figure 5: Zygotic *prox1a* mutants display a unique chromatin accessibility state in fate-shifted endothelial cells

a. Heatmaps of accessibility (gene score) for all genes (n=32 020 genes) in WT LECs, WT VECs and Mutant Cluster showing that mutant cluster cells display a unique chromatin state at many genes.

784 **b.** Schematic illustrates DAP analyses between Mutant Cluster vs. LEC WT and Mutant
785 Cluster vs. VEC WT. Venn diagram indicates all individual peaks that were found to be
786 increased in accessibility in the Mutant Cluster vs LEC or VEC with n=431 DAP
787 commonly more open than in both LEC WT and VEC WT (FDR < 0.05, log2 fold change
788 > 1.5).
789 **c.** Dot plot summarizing the scRNA-seq expression level of n=13 genes with DAP more
790 open in the Mutant Cluster at 4dpf, demonstrating that accessibility changes for these
791 genes did not correlate with changes in transcription. The size of the dot represents
792 the proportion of cells that express the markers in the cluster, and colour represents
793 SCT-normalised expression.
794 **d.** Top 10 enriched motifs (HOMER analysis, adjusted p value < 0.05) in the n=431 peaks
795 that are more open in the Mutant Cluster than WT LEC and VEC. Percentages on the
796 right-hand side represent the proportion of regions enriched for the motif in the
797 n=431 peak set, and the whole genome (background).
798 **e.** Genome accessibility track of *prox1a*. Red bars represent peaks in the reproducible
799 peak set from snATAC-seq.
800 **f.** Genome accessibility track of *tbx1*. Red bars represent peaks in the reproducible peak
801 set from snATAC-seq
802 **g.** Genome accessibility track of *kdr*. Red bars represent peaks in the reproducible peak
803 set from snATAC-seq
804
805 DAP, differentially accessible peaks. FDR, false discovery rate. snATAC-seq, single nuclei
806 ATAC-seq.
807

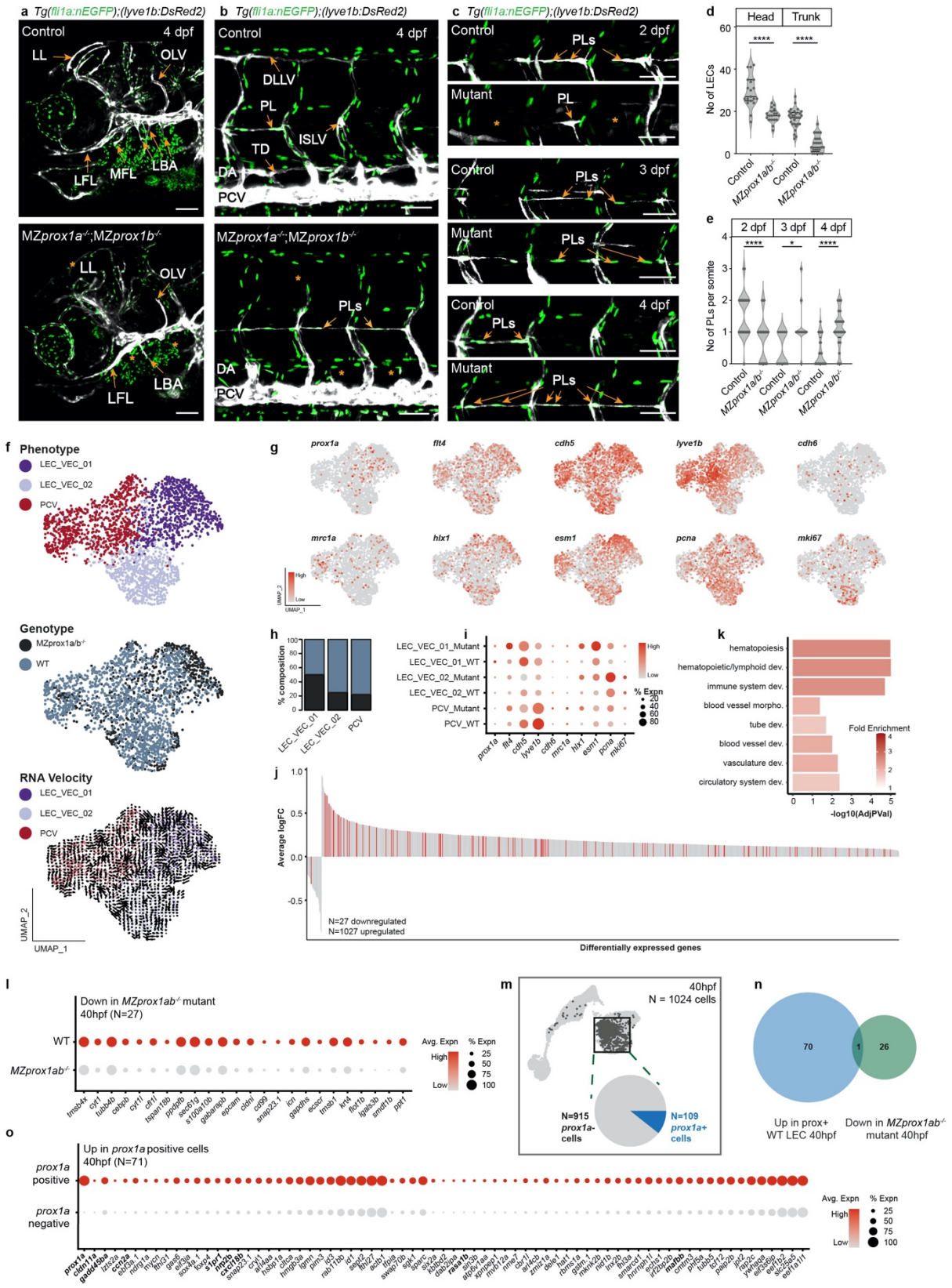

Figure 6: The role of Prox1 in LEC specification and sprouting revealed by single cell profiling of maternal zygotic *prox1a;prox1b* double mutants

811 **a.** Lateral confocal images of zebrafish heads at 4dpf showing endothelial cell nuclei
812 (green) and venous and lymphatic vessels (white) in control (upper) and *MZprox1a*$^{-/-}$
813 *;MZprox1b*$^{-/-}$ embryos (lower). Facial lymphatics are absent or shorter or missing
814 (asterisk) in the mutants (asterisk). Scale bar, 80 µm.
815 **b.** Lateral confocal images of zebrafish trunks at 4dpf in control (upper) and *MZprox1a*$^{-/-}$
816 *;MZprox1b*$^{-/-}$ mutants (lower), showing absent lymphatic vessels (asterisk) but
817 retained PLs (arrows in lower). Scale bars, 50 µm.
818 **c.** Lateral confocal images of PLs in the horizontal myoseptum at 2, 3 and 4dpf. PLs form
819 later in *MZprox1a*$^{-/-}$*;MZprox1b*$^{-/-}$ mutants and accumulate in the horizontal
820 myoseptum while the PLs of control embryos emigrate the HM by 4dpf. Scale bars,
821 50 µm.
822 **d.** Quantification of lymphatic endothelial cell (LEC) number from 4dpf heads control:
823 n=19, *MZprox1a*$^{-/-}$*;MZprox1b*$^{-/-}$ mutants: n=18) and trunks (control: n=29, *MZprox1a*$^{-/-}$
824 *;MZprox1b*$^{-/-}$ mutants:n=25). Error bars represent mean ± s.e.m.; **** $p < 0.0001$,
825 from an unpaired, two-sided t-test.
826 **e.** Quantification of number of PLs per somite in trunks at 2dpf in controls (n=41) and
827 *MZprox1a*$^{-/-}$*;MZprox1b*$^{-/-}$ mutants (n=38), at 3dpf in controls (n=11) and *MZprox1a*$^{-/-}$
828 *;MZprox1b*$^{-/-}$ mutants (n=10) and at 4dpf in controls (n=29) and *MZprox1a*$^{-/-}$
829 *;MZprox1b*$^{-/-}$ mutants (n=25). Error bars represent mean ± s.e.m.; **** $p < 0.0001$, *
830 $p < 0.05$, from an unpaired, two-sided t-test.
831 **f.** UMAP visualization of filtered scRNA-seq data showing 2202 endothelial cells (n=4
832 samples; **Extended data table 6a**) coloured according to predicted cell phenotype
833 (top), genotype (middle), and RNA-velocity (bottom).
834 **g.** UMAP visualization of key marker gene expression. Colour scale represents SCT-
835 normalised expression.
836 **h.** Stacked bar plot representing the genotype composition of cells in each cluster.
837 **i.** Dot plot of key marker expression. Colour scale represents average SCT-normalised
838 expression and point size represents percentage of cells expressing gene.
839 **j.** Bar plot indicating average log fold change of n=1054 significantly different genes
840 between the *MZprox1a/b*$^{-/-}$ and WT cells in LEC_VEC_01 and LEC_VEC_02 clusters at
841 40hpf (Wilcoxin Rank Sum *adjusted p value* < 0.05).

842 **k.** Bar plot summarizing GO BP analyses of n=1027 genes upregulated in *MZprox1a/b*$^{-/-}$.
843 Y-axis represents enriched BP term, x-axis represents the -log10(*adjusted p value*),
844 bars are coloured according to fold enrichment.
845 **l.** Dot plot of n=27 genes downregulated in 40hpf *MZprox1a/b*$^{-/-}$ and WT cells in
846 LEC_VEC_01 and LEC_VEC_02 clusters.
847 **m.** Schematic outlining the selection of n=109 *prox1a* expressing cells from n=915 *prox1a*
848 negative counterparts in the 40hpf WT sample (whole dataset in **Fig1**). DEG analysis
849 revealed n=71 genes upregulated in *prox1a* positive cells (Wilcoxin Rank Sum *adjusted*
850 *p value* < 0.05).
851 **n.** Venn diagram illustrating genes upregulated in *prox1a* positive (vs negative) WT cells
852 at 40hpf, and downregulated in *MZprox1a/b*$^{-/-}$ mutant cells at 40hpf.
853 **o.** Dot plot of n=71 genes upregulated in WT *prox1a* positive (vs negative) cells at 40hpf.
854 Colour scale represents average SCT-normalised expression and point size represents
855 percentage of cells expressing gene. Bold labels indicate known lymphatic genes.
856
857 LL, lymphatic loop. OLV, otholitic lymphatic vessel. LFL, lateral facial lymphatic vessel. MFL,
858 medial facial lymphatic vessel. LBA, lymphatic branchial arches. DLLV, dorsal longitudinal
859 lymphatic vessel. PL, parachordal LEC. ISLV, intersomitic lymphatic vessel. TD, thoracic duct.
860 DA, dorsal aorta. PCV, posterior cardinal vein.
861

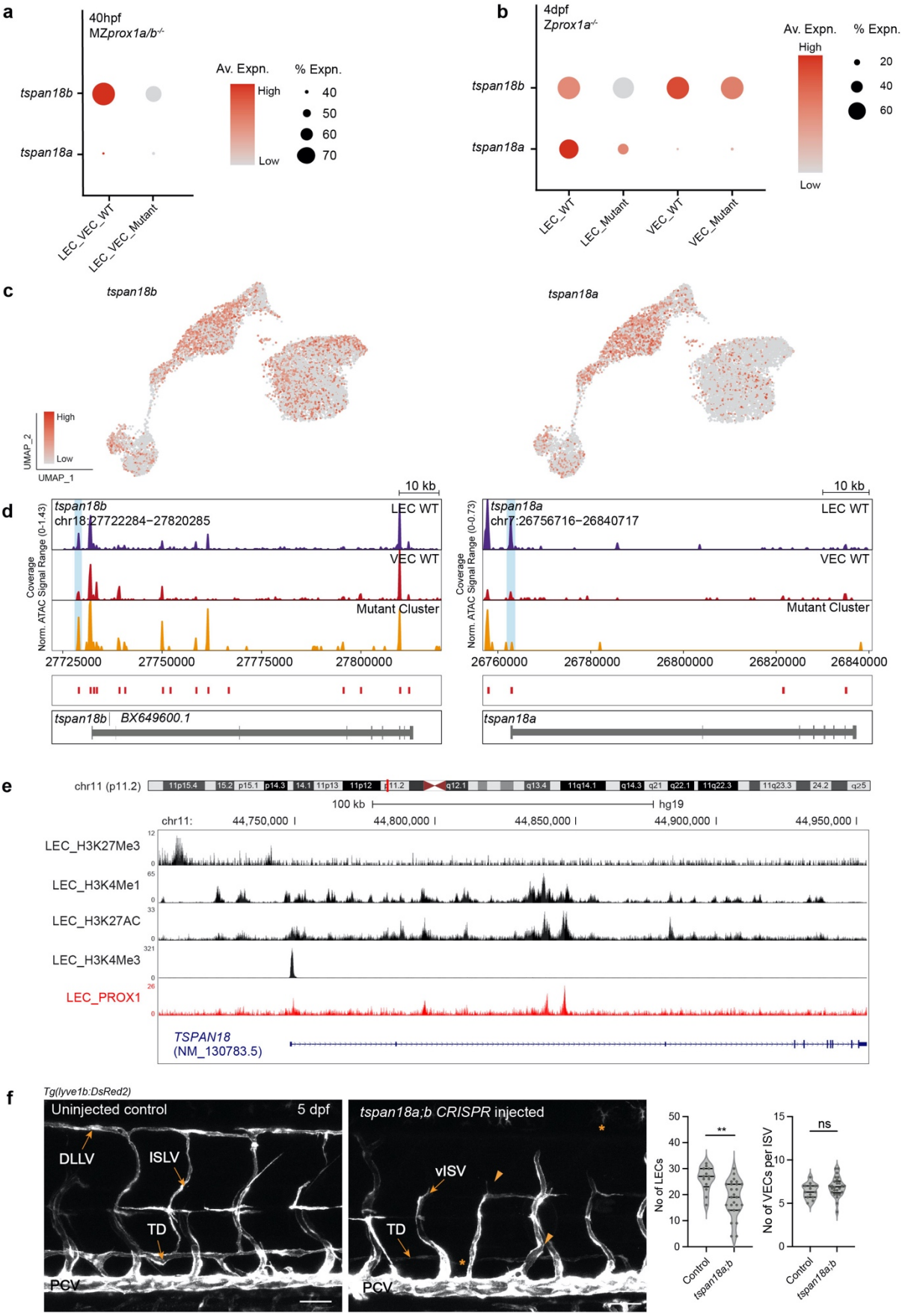
a
40hpf
MZprox1a/b-/-
tspan18b
tspan18a
Av. Expn.
High
Low
% Expn.
40
50
60
70
LEC_VEC_WT
LEC_VEC_Mutant
b
4dpf
Zprox1a-/-
tspan18b
tspan18a
Av. Expn.
High
Low
% Expn.
20
40
60
LEC_WT
LEC_Mutant
VEC_WT
VEC_Mutant
c
tspan18b
tspan18a
High
Low
UMAP_2
UMAP_1
d
10 kb
tspan18b
chr18:27722284–27820285
LEC WT
VEC WT
Mutant Cluster
Coverage
Norm. ATAC Signal Range (0-1.43)
27725000
27750000
27775000
27800000
tspan18b
BX649600.1
tspan18a
chr7:26756716–26840717
Norm. ATAC Signal Range (0-0.73)
26760000
26780000
26800000
26820000
26840000
tspan18a
e
chr11 (p11.2)
100 kb
hg19
chr11:
44,750,000
44,800,000
44,850,000
44,900,000
44,950,000
LEC_H3K27Me3
LEC_H3K4Me1
LEC_H3K27AC
LEC_H3K4Me3
LEC_PROX1
TSPAN18
(NM_130783.5)
f
Tg(lyve1b:DsRed2)
Uninjected control
5 dpf
DLLV
ISLV
TD
PCV
tspan18a;b CRISPR injected
vISV
TD
PCV
No of LECs
**
Control
tspan18a;b
No of VECs per ISV
ns
Control
tspan18a;b

862

863 **Figure 7: Identification of Tspan18 paralogues as functionally essential downstream targets**
864 **of Prox1 in lymphangiogenesis**

865 **a.** Dot plot of expression of *tspan18b* and *tspan18a* in WT and *MZprox1a/b*$^{-/-}$ mutant cells
866 at 40hpf. The size of the dot represents the proportion of cells that express the
867 markers in the cluster, and colour represents SCT-normalised expression.

868 **b.** Dot plot of expression of *tspan18b* and *tspan18a* in Wt and *Zprox1a*$^{-/-}$ mutant cells at
869 4dpf. The size of the dot represents the proportion of cells that express the markers
870 in the cluster, and colour represents SCT-normalised expression.

871 **c.** UMAP visualization of *tspan18b* and *tspan18a* expression in the single cell atlas of
872 lymphangiogenesis. Colour scale represents log-normalised expression.

873 **d.** Genome accessibility track of *tspan18b* (left) and *tspan18a* (right). Red bars represent
874 peaks in the reproducible peak set from snATAC-seq. Differentially accessible peaks
875 between Mutant Cluster and WT LECs (*p value* < 0.05) were highlighted in blue

876 **e.** ChIP-seq profile of Prox1 binding together with H3K27Me3, H3K4Me1, H3K27AC, and
877 H3K4Me3 profiles at the TSPAN18 locus (hg19) in human LECs.

878 **f.** Lateral confocal images of zebrafish trunks depicting mature lymphatic vessels in the
879 uninjected control which are missing in tspan18a;b CRISPR injected embryos at 5dpf
880 (asterisks) identifying a functional requirement for tspan18 paralogues in
881 lymphangiogenesis. Note that the formation of intersegmental vessels is also severely
882 impaired in tspan18a;b crispants (arrowheads).. Scale bars, 50 µm. Quantification of
883 LEC numbers across 4 somites and VEC numbers per vISV at 5dpf. Error bars represent
884 mean ± s.e.m.; ** p = 0.0012, ns = not significant from an unpaired, two-sided t-test.

885

886 DLLV, dorsal longitudinal lymphatic vessel. ISLV, intersomitic lymphatic vessel. TD, thoracic
887 duct. PCV, posterior cardinal vein. vISV, venous intersegmental vessel.

EXTENDED DATA FIGURES AND FIGURE LEGENDS

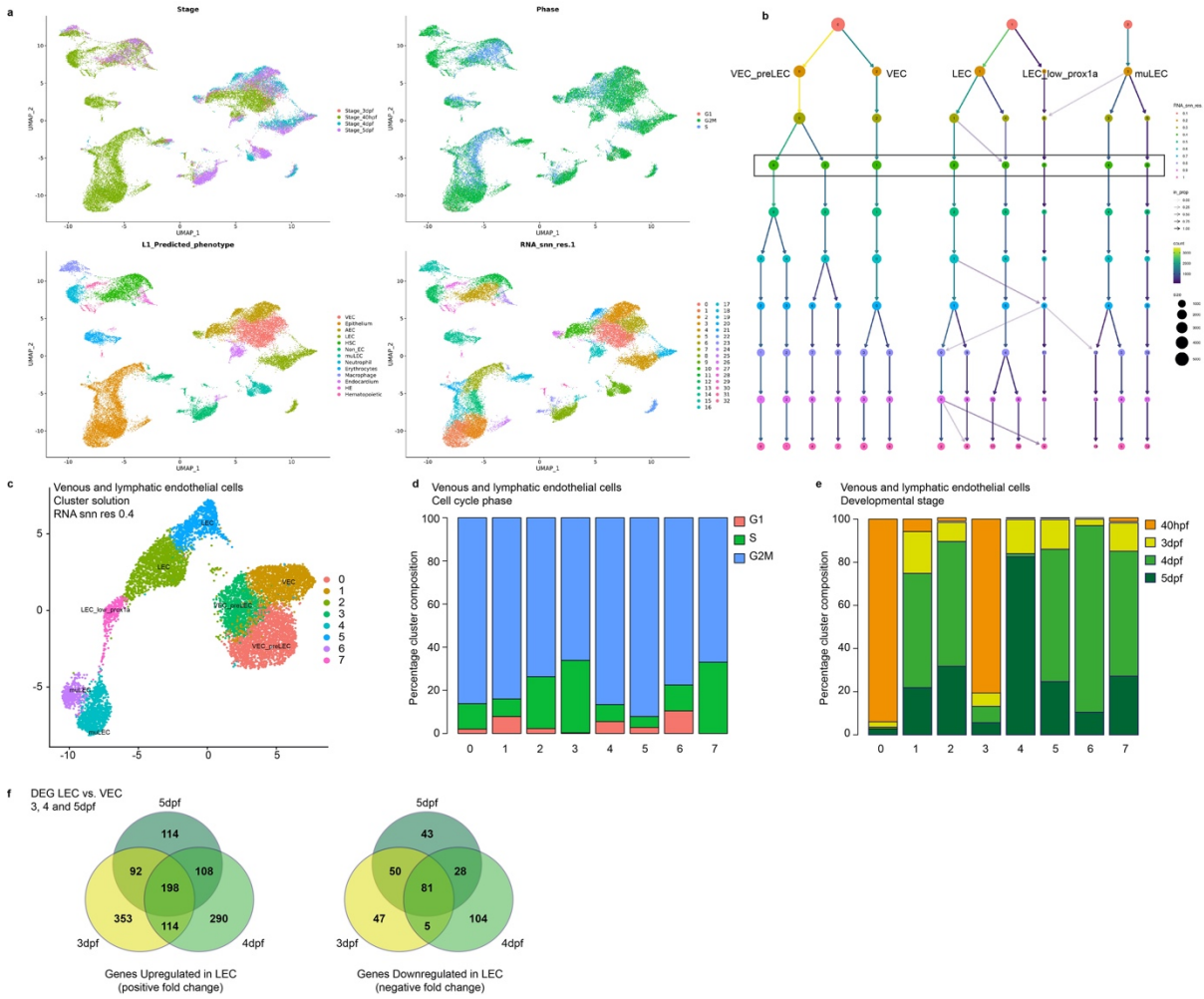

Extended data Fig 1: Full dataset and analysis for data in Fig 1.

- **a.** UMAP visualization of n=35634 endothelial cells sequenced for the single cell atlas of lymphangiogenesis (n=6 samples; see also **Extended data table 1a** for markers used to identify clusters) coloured according to developmental stage (top left), cell cycle phase (top right), predicted cell phenotype (bottom left), and cluster solution (RNA-snn-res.1).
- **b.** Clustree analysis demonstrating the relationship between different cluster resolutions for the n=9771 venous and lymphatic endothelial cells in Figure 1a. Resolution 0.4 (boxed) was used for all downstream analyses.
- **c.** UMAP visualization of cluster resolution 0.4 (as appears in **Fig 1**).
- **d.** Stacked bar plot of resolution 0.4 cluster composition cell cycle phase.
- **e.** Stacked bar plot of resolution 0.4 cluster composition developmental stage.

902 **f.** Venn diagram of significant genes commonly upregulated in LEC compared to VEC at
903 3, 4 and 5dpf.
904

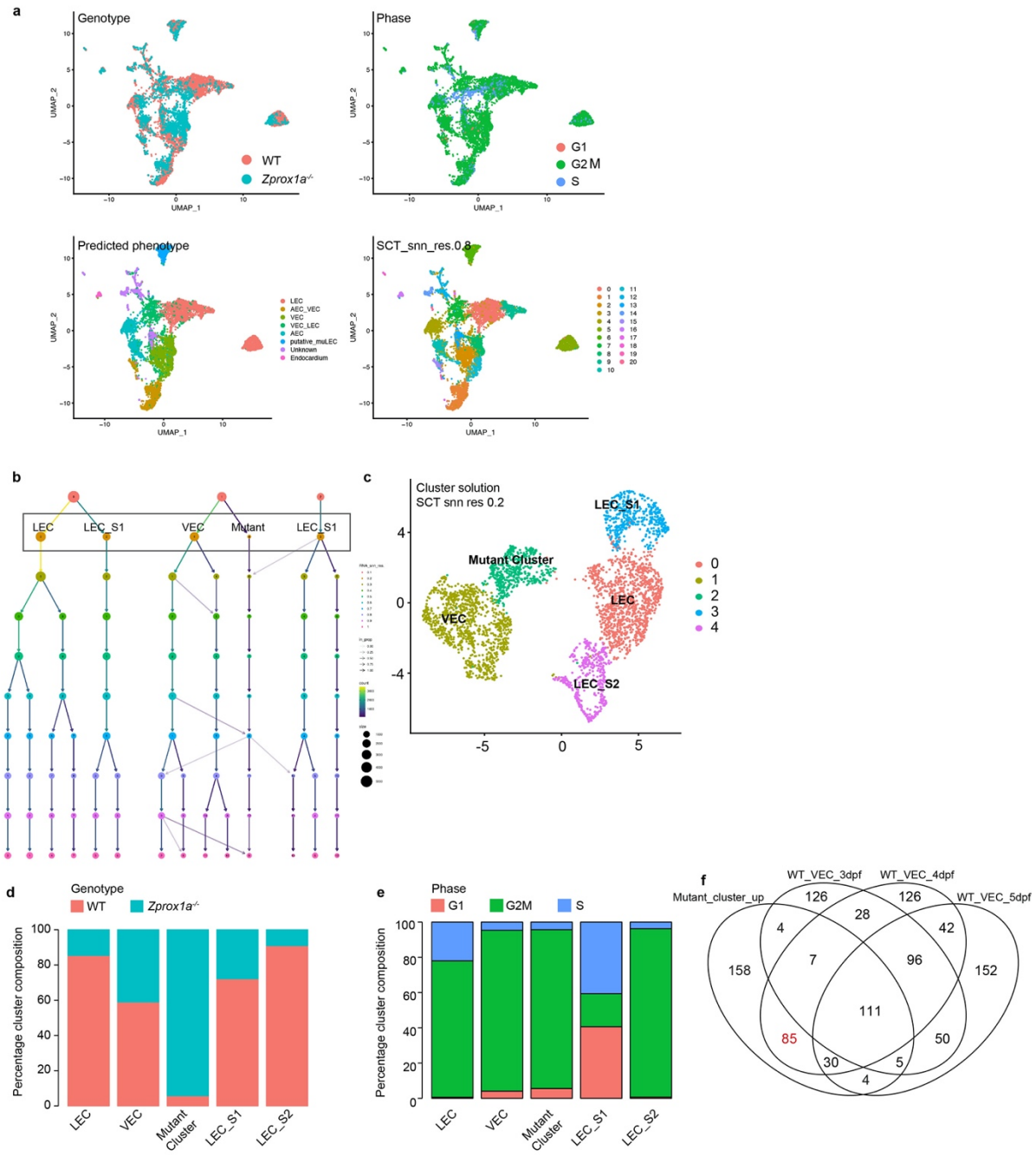

Extended data Fig 2: Full dataset and analysis for data in Fig 3.

a. UMAP visualization of n=8075 endothelial cells sequenced comparing lymphangiogenesis in WT and *Zprox1a* mutants at 4dpf (n=2 samples; see also **Extended data table 2a** for markers used to identify clusters) coloured according to developmental stage (top left), cell cycle phase (top right), predicted cell phenotype (bottom left), and cluster solution (SCT-snn-res.8)

912 **b.** Clustree analysis demonstrating the relationship between different cluster resolutions
913 for the n=3063 venous and lymphatic endothelial cells in **Figure 3a**. Resolution 0.2
914 (boxed) was used for all downstream analyses.
915 **c.** UMAP visualization of cluster resolution 0.2
916 **d.** Stacked bar plot of resolution 0.2 cluster composition genotype
917 **e.** Stacked bar plot of resolution 0.2 cluster composition cell cycle phase
918 **f.** Venn diagram indicates the overlap between genes significantly upregulated in VEC
919 compared to LEC at each developmental stage of the single cell atlas, and those
920 upregulated in the *Zprox1a*$^{-/-}$ Mutant Cluster at 4dpf compared to WT LECs. N=85
921 genes (coloured red) are uniquely associated with the Mutant Cluster and WT VEC at
922 4dpf, compared to N=4 genes in WT VEC at 3 and 5dpf.
923

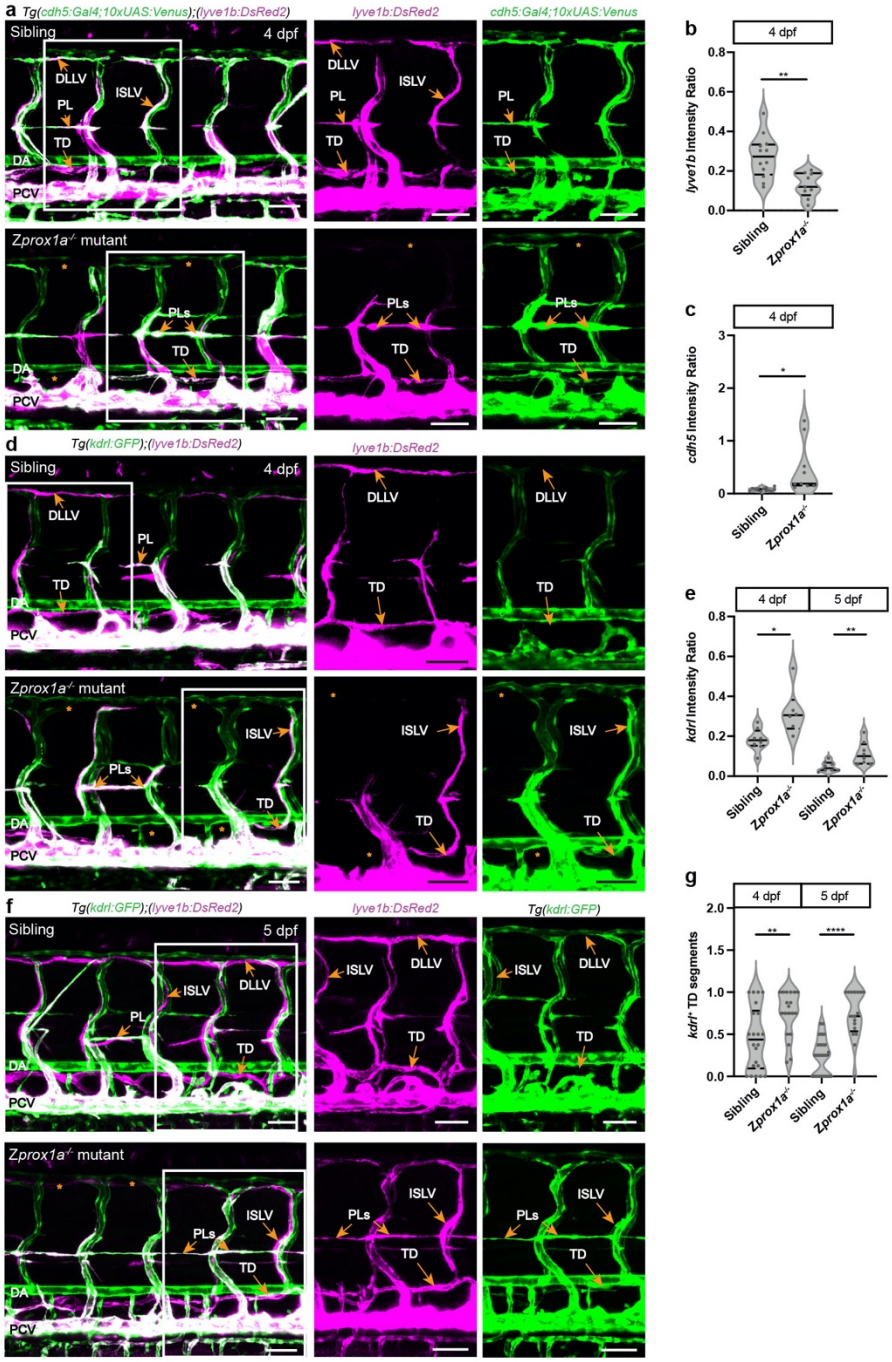

Extended data Fig 3: Additional phenotypic analysis of blood vascular markers in *Zprox1a*$^{-/-}$ mutants associated with Fig 3

a. Lateral confocal images of zebrafish trunks at 4dpf showing *cdh5* expression (green) and *lyve1b* expression in lymphatic vessels (magenta) in control (upper) and *Zprox1a* mutant embryos (lower). Transgenic lines are indicated. Scale bar, 50 µm.

b. Quantification of *lyve1b* expression intensity in the TD relative to the PCV in sibling and *Zprox1a* mutant embryos at 4dpf.

932 **c.** Quantification of *cdh5* expression intensity in the TD relative to the DA in sibling and
933 *Zprox1a* mutant embryos at 4dpf.
934 **d.** Lateral confocal images of zebrafish trunks at 4dpf showing *kdrl* expression (green)
935 and *lyve1b* expression in lymphatic vessels (magenta) in control (upper) and *Zprox1a*
936 mutants (lower). Transgenic lines are indicated. Scale bars, 50 µm.
937 **e.** Quantification of *kdrl* expression intensity in the TD relative to the DA in sibling and
938 *Zprox1a* mutant embryos at 4dpf and 5dpf (upper).
939 **f.** Lateral confocal images of zebrafish trunks at 5dpf showing *kdrl* expression (green)
940 and *lyve1b* expression in lymphatic vessels (magenta) in control (upper) and *Zprox1a*
941 mutants (lower). Transgenic lines are indicated. Scale bars, 50 µm.
942 **g.** Quantification of the number of TD segments displaying *kdrl* expression in *Zprox1a*
943 mutant embryos at 4dpf and 5dpf (lower).
944 DLLV, dorsal longitudinal lymphatic vessel. ISLV, intersomitic lymphatic vessel. TD, thoracic
945 duct. DA, Dorsal aorta. PCV, posterior cardinal vein. vISV, venous intersegmental vessel. PL,
946 Parachoral lymphatic endothelial cells.
947

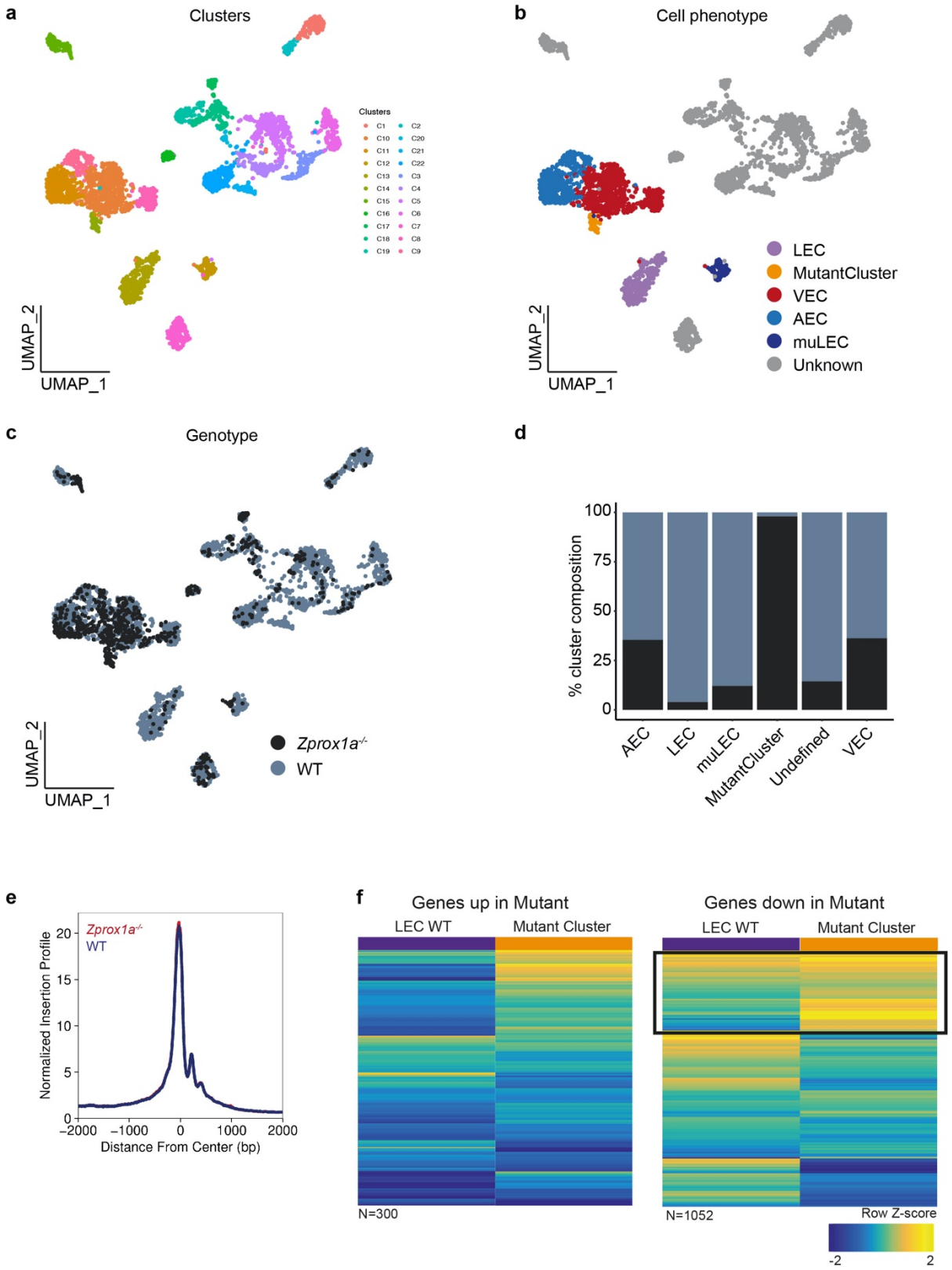

Extended data Fig 4: Additional data and analysis for data in Fig 4.

a. UMAP visualization of n=3731 single nuclei ATAC-seq data comparing lymphangiogenesis in WT and *Zprox1a* mutants at 4dpf. Nuclei coloured according to cluster (res-0.8).

953 **b.** UMAP visualisation with nuclei coloured according to predicted phenotype based on
954 accessibility changes at the genes defined in **Extended data table 1c.**
955 **c.** UMAP visualisation with nuclei coloured according to genotype.
956 **d.** Stacked bar plot indicating the genotype composition of nuclei captured per cell type.
957 **e.** Density plot indicating the majority of snATAC-seq peaks fall around the TSS. Y-axis
958 represents distance from TSS (bp) and y-axis represents normalised Tn5 insertion
959 profile.
960 **f.** Heatmaps of accessibility (gene score) for DEG (**Fig 3f**) upregulated (left, n=300
961 mapped genes) and downregulated (right, n=1052 mapped genes) in the Mutant
962 Cluster compared to WT LECs. Colour indicates row-wise Z-score, each row represents
963 a differentially expressed gene in scRNA-seq data, columns are snATAC-seq clusters.
964 Boxed genes downregulated in Mutant display more permissive chromatin in Mutant
965 than WT LEC, showing that mutant cluster cells display a unique chromatin state at
966 many genes.
967

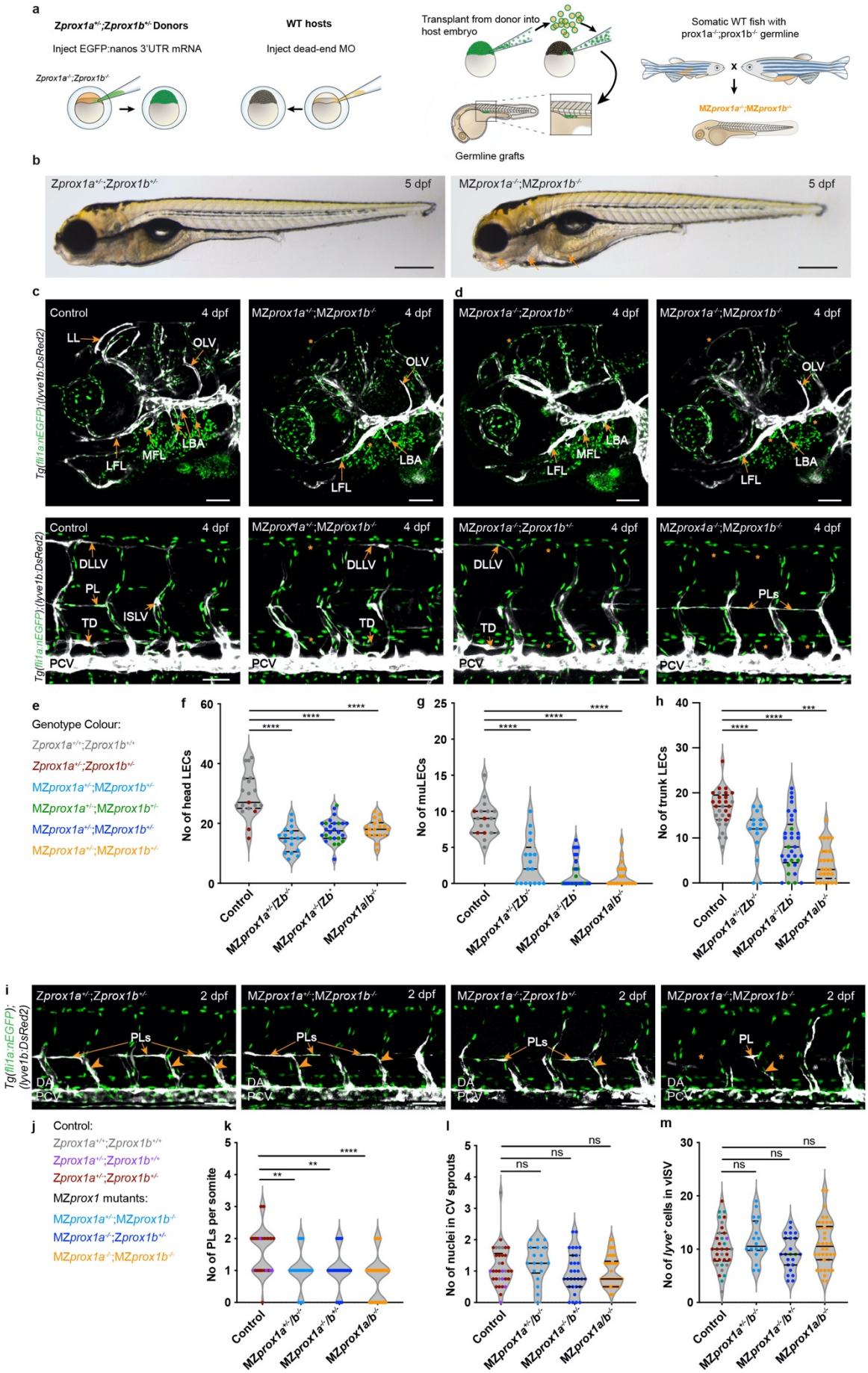
a
Zprox1a+/-;Zprox1b+/- Donors
Inject EGFP:nanos 3'UTR mRNA
WT hosts
Inject dead-end MO
Transplant from donor into host embryo
Germline grafts
Somatic WT fish with prox1a-/-;prox1b-/- germline
MZprox1a-/-;MZprox1b-/-
b
Zprox1a+/-;Zprox1b+/-
5 dpf
MZprox1a-/-;MZprox1b-/-
5 dpf
c
d
Control
4 dpf
MZprox1a+/-;MZprox1b-/-
MZprox1a-/-;Zprox1b+/-
MZprox1a-/-;MZprox1b-/-
Tg(fli1a:nEGFP);(lyve1b:DsRed2)
LL
OLV
LFL
MFL
LBA
DLLV
PL
ISLV
TD
PCV
PLs
e
Genotype Colour:
Zprox1a+/+;Zprox1b+/+
Zprox1a+/-;Zprox1b+/-
MZprox1a+/-;MZprox1b+/-
MZprox1a+/-;MZprox1b+/-
MZprox1a+/-;MZprox1b+/-
MZprox1a+/-;MZprox1b+/-
f
No of head LECs
g
No of muLECs
h
No of trunk LECs
Control
MZprox1a+/-/Zb-/-
MZprox1a-/-/Zb+
MZprox1a/b-/-
i
Zprox1a+/-;Zprox1b+/-
2 dpf
MZprox1a+/-;MZprox1b-/-
MZprox1a-/-;Zprox1b+/-
MZprox1a-/-;MZprox1b-/-
Tg(fli1a:nEGFP);(lyve1b:DsRed2)
PLs
PL
DA
PCV
j
Control:
Zprox1a+/+;Zprox1b+/+
Zprox1a+/-;Zprox1b+/+
Zprox1a+/-;Zprox1b+/-
MZprox1 mutants:
MZprox1a+/-;MZprox1b-/-
MZprox1a-/-;Zprox1b+/-
MZprox1a-/-;MZprox1b-/-
k
No of PLs per somite
l
No of nuclei in CV sprouts
m
No of lyve+ cells in vISV
ns

969 **Extended data Fig 5**: **Additional phenotypic analysis of *MZprox1a*$^{-/-}$;*MZprox1b*$^{-/-}$ mutants**
970 **associated with Fig 6**

971 **a.** Schematic explanation of the germline replacement transplantation method used to
972 generate *MZprox1a*$^{-/-}$;*MZprox1b*$^{-/-}$ mutants.

973 **b.** Overall morphology of control and *MZprox1a*$^{-/-}$;*MZprox1b*$^{-/-}$ mutants at 5dpf. Arrows
974 indicate oedema around eyes, heart and intestine. Scale bars 500 µm.

975 **c-d.** Lateral confocal images showing vascular defects in control and mutant in the craniofacial
976 (**c**) and trunk (**d**) regions of the larvae at 4dpf. Genotypes and transgenic labels are indicated.
977 *MZprox1a-/-* and *MZprox1a+/-, MZprox1b-/-* animals both showed a strong loss of lymphatic
978 vessels in craniofacial and trunk regions. The *MZprox1a-/-, MZprox1a-/-* mutants showed a
979 robust loss of craniofacial vessels equivalent to the other mutant phenotypes but a more
980 severe loss of trunk lymphatics and an accumulation of PLs in the HM.

981 **e.** Genotypes that are shown in the quantification. Colour codes are used to identify
982 individual embryonic genotypes in the dot plots showing quantification in **f-h**.

983 **f.** Quantification of the number of craniofacial (head) LECs within facial lymphatic
984 vessels showing evidence for contributions from *prox1a* and *prox1b*.

985 **g.** Quantification of the number of mural LECs (muLECs) showing a major role for *prox1a*
986 and a role for *prox1b* in muLEC development.

987 **h.** Quantification of the number of trunk LECs within vessels showing a dominant role for
988 *prox1a* in trunk lymphangiogenesis.

989 **i.** Lateral confocal images showing defects in the formation of PLs in mutants upon loss
990 of *prox1a* compared with controls in the trunk. Genotypes are indicated.

991 **j.** Colour coded list of analysed genotypes abbreviated in (**k-m**). Each embryo has a
992 defined genotype for *prox1b* which is represented in colour code as displayed in j.

993 **k.** The number of PLs formed (per somite) at 2dpf in genotypes indicated. Decreasing
994 gene dosage for *prox1a* and *prox1b* progressively reduced the initial seeding of the
995 HM by PLs.

996 **l.** The number of cells in sprouts departing the PCV is unchanged in mutants showing
997 that sprouting occurs normally.

998 **m.** The number of cells in vISVs is unchanged in mutants indicating no effect on the
999 venous endothelium.

Z, zygotic; MZ, maternal and zygotic; HM, horizontal myoseptum; LL, lymphatic loop; OLV, otholitic lymphatic vessel; LFL, lateral facial lymphatic vessel; MFL, medial facial lymphatic vessel; LBA, lymphatic branchial arches; DLLV, dorsal longitudinal lymphatic vessel; PL, parachordal LEC; ISLV, intersomitic lymphatic vessel; TD, thoracic duct; DA, dorsal aorta; PCV, posterior cardinal vein.

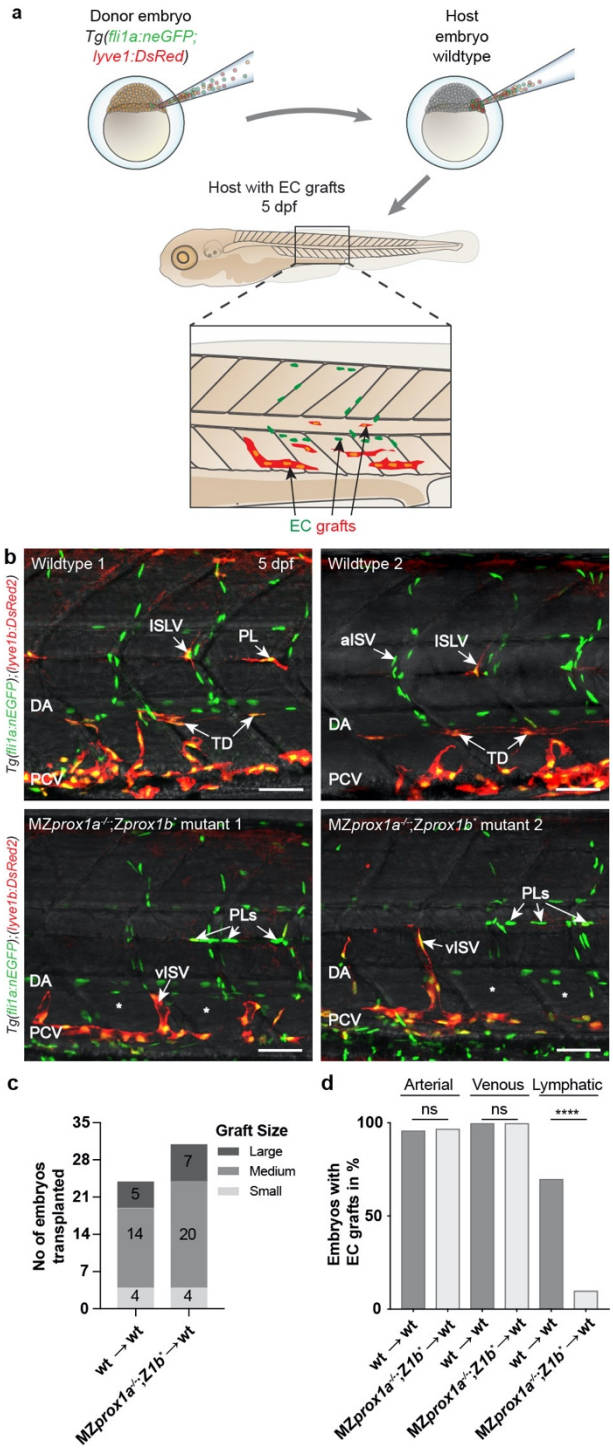

Extended data Fig 6: **Embryonic transplantation data demonstrating endothelial cell autonomy of *prox1a* maternal zygotic mutant phenotype associated with Fig 6.**

a. Schematic showing the endothelial cell transplantation approach used to test cell autonomy for the vascular phenotypes seen in *MZprox1a* mutants. Cell identities were traced following transplantation in unlabelled host embryos using expression of the pan -endothelial marker *fli1a* and venous/lymphatic marker *lyve1b* (indicated).

1013 **b.** Examples of 5dpf wildtype hosts engrafted with wildtype donor cells (upper) that
1014 contribute to arteries (aISVs, DA), veins (PCV, vISVs) and lymphatic vessels (TD, ISLVs)
1015 and examples of wildtype embryos engrafted with *MZprox1a* mutant cells
1016 contributing arteries (aISVs, DA) and veins (vISV, PCV) but not lymphatic vessels. Note
1017 the PL accumulation in the horizontal myoseptum..
1018 **c.** The number of embryos imaged and graft sizes scored post-tranplantation. As the
1019 contribution to the different EC types is affected by the graft size, we analysed grafts
1020 of comparable sizes and position from wildtype and mutant embryos. Grafts were
1021 categorised as large, medium or small. Small (spanning 1-2 somites), medium
1022 (spanning 2-3 somites) and large grafts (spanning 4-5 somites). The number of ECs
1023 contributing to each EC type was scored at single cell resolution and the percentage
1024 of grafts with a contribution to each lineage calculated accordingly. The numbers
1025 within the different graft groups indicate the number of analysed embryos within that
1026 group.
1027 **d.** The percentage of embryos with vascular grafts that display contributions to arteries,
1028 veins and lymphatics. *MZprox1a*$^{-/-}$ mutant cells contribute to arteries and veins but
1029 showed a near complete loss of contribution to lymphatics. The size of the grafts did
1030 not influence the outcome. *Z1b** indicates a mixed prox1b background. $p < 0.0001$
1031 from an unpaired, two-sided t-test.
1032 DA, dorsal aorta. PCV, posterior cardinal vein. PL, parachordal LEC. TD, thoracic duct. aISV,
1033 arterial intersegmental vessel. vISV, venous intersegmental vessel. ISLV, intersegmental
1034 lymphatic vessel.
1035

1036 **References**

1037 1 Oliver, G., Kipnis, J., Randolph, G. J. & Harvey, N. L. The Lymphatic Vasculature in
1038 the 21(st) Century: Novel Functional Roles in Homeostasis and Disease. *Cell* **182**,
1039 270-296, doi:10.1016/j.cell.2020.06.039 (2020).
1040 2 Koltowska, K., Betterman, K. L., Harvey, N. L. & Hogan, B. M. Getting out and
1041 about: the emergence and morphogenesis of the vertebrate lymphatic vasculature.
1042 *Development* **140**, 1857-1870, doi:10.1242/dev.089565 (2013).
1043 3 Baek, S. *et al.* The Alternative Splicing Regulator Nova2 Constrains Vascular Erk
1044 Signaling to Limit Specification of the Lymphatic Lineage. *Dev Cell* **49**, 279-292
1045 e275, doi:10.1016/j.devcel.2019.03.017 (2019).
1046 4 Koltowska, K. *et al.* Vegfc Regulates Bipotential Precursor Division and Prox1
1047 Expression to Promote Lymphatic Identity in Zebrafish. *Cell Rep* **13**, 1828-1841,
1048 doi:10.1016/j.celrep.2015.10.055 (2015).
1049 5 Deng, Y., Atri, D., Eichmann, A. & Simons, M. Endothelial ERK signaling controls
1050 lymphatic fate specification. *The Journal of clinical investigation* **123**, 1202-1215,
1051 doi:10.1172/JCI63034 (2013).
1052 6 Shin, M. *et al.* Vegfc acts through ERK to induce sprouting and differentiation of
1053 trunk lymphatic progenitors. *Development* **143**, 3785-3795, doi:10.1242/dev.137901
1054 (2016).
1055 7 Srinivasan, R. S. *et al.* The Prox1-Vegfr3 feedback loop maintains the identity and the
1056 number of lymphatic endothelial cell progenitors. *Genes Dev* **28**, 2175-2187,
1057 doi:10.1101/gad.216226.113 (2014).
1058 8 Oliver, G. & Srinivasan, R. S. Endothelial cell plasticity: how to become and remain a
1059 lymphatic endothelial cell. *Development* **137**, 363-372, doi:10.1242/dev.035360
1060 (2010).
1061 9 Wigle, J. T. & Oliver, G. Prox1 function is required for the development of the
1062 murine lymphatic system. *Cell* **98**, 769-778, doi:10.1016/s0092-8674(00)81511-1
1063 (1999).
1064 10 Hagerling, R. *et al.* A novel multistep mechanism for initial lymphangiogenesis in
1065 mouse embryos based on ultramicroscopy. *The EMBO journal* **32**, 629-644,
1066 doi:10.1038/emboj.2012.340 (2013).
1067 11 Klotz, L. *et al.* Cardiac lymphatics are heterogeneous in origin and respond to injury.
1068 *Nature* **522**, 62-67, doi:10.1038/nature14483 (2015).
1069 12 Martinez-Corral, I. *et al.* Nonvenous origin of dermal lymphatic vasculature. *Circ Res*
1070 **116**, 1649-1654, doi:10.1161/CIRCRESAHA.116.306170 (2015).
1071 13 Stanczuk, L. *et al.* cKit Lineage Hemogenic Endothelium-Derived Cells Contribute to
1072 Mesenteric Lymphatic Vessels. *Cell Rep* **10**, 1708-1721,
1073 doi:10.1016/j.celrep.2015.02.026 (2015).
1074 14 Srinivasan, R. S. *et al.* Lineage tracing demonstrates the venous origin of the
1075 mammalian lymphatic vasculature. *Genes Dev* **21**, 2422-2432,
1076 doi:10.1101/gad.1588407 (2007).
1077 15 Srinivasan, R. S. *et al.* The nuclear hormone receptor Coup-TFII is required for the
1078 initiation and early maintenance of Prox1 expression in lymphatic endothelial cells.
1079 *Genes Dev* **24**, 696-707, doi:10.1101/gad.1859310 (2010).
1080 16 Yang, Y. *et al.* Lymphatic endothelial progenitors bud from the cardinal vein and
1081 intersomitic vessels in mammalian embryos. *Blood* **120**, 2340-2348,
1082 doi:10.1182/blood-2012-05-428607 (2012).

17 Stone, O. A. & Stainier, D. Y. R. Paraxial Mesoderm Is the Major Source of Lymphatic Endothelium. *Dev Cell* **50**, 247-255 e243, doi:10.1016/j.devcel.2019.04.034 (2019).

18 Johnson, N. C. *et al.* Lymphatic endothelial cell identity is reversible and its maintenance requires Prox1 activity. *Genes Dev* **22**, 3282-3291, doi:10.1101/gad.1727208 (2008).

19 Tao, S. *et al.* Zebrafish prox1b mutants develop a lymphatic vasculature, and prox1b does not specifically mark lymphatic endothelial cells. *PLoS One* **6**, e28934, doi:10.1371/journal.pone.0028934 (2011).

20 van Impel, A. *et al.* Divergence of zebrafish and mouse lymphatic cell fate specification pathways. *Development* **141**, 1228-1238, doi:10.1242/dev.105031 (2014).

21 Hogan, B. M. *et al.* Ccbe1 is required for embryonic lymphangiogenesis and venous sprouting. *Nat Genet* **41**, 396-398, doi:10.1038/ng.321 (2009).

22 Yaniv, K. *et al.* Live imaging of lymphatic development in the zebrafish. *Nat Med* **12**, 711-716, doi:10.1038/nm1427 (2006).

23 Eng, T. C. *et al.* Zebrafish facial lymphatics develop through sequential addition of venous and non-venous progenitors. *EMBO Rep* **20**, doi:10.15252/embr.201847079 (2019).

24 Okuda, K. S. *et al.* lyve1 expression reveals novel lymphatic vessels and new mechanisms for lymphatic vessel development in zebrafish. *Development* **139**, 2381-2391, doi:10.1242/dev.077701 (2012).

25 Bussmann, J. *et al.* Arteries provide essential guidance cues for lymphatic endothelial cells in the zebrafish trunk. *Development* **137**, 2653-2657, doi:10.1242/dev.048207 (2010).

26 Cha, Y. R. *et al.* Chemokine signaling directs trunk lymphatic network formation along the preexisting blood vasculature. *Dev Cell* **22**, 824-836, doi:10.1016/j.devcel.2012.01.011 (2012).

27 Jung, H. M. *et al.* Development of the larval lymphatic system in zebrafish. *Development* **144**, 2070-2081, doi:10.1242/dev.145755 (2017).

28 Bower, N. I. *et al.* Mural lymphatic endothelial cells regulate meningeal angiogenesis in the zebrafish. *Nat Neurosci* **20**, 774-783, doi:10.1038/nn.4558 (2017).

29 van Lessen, M. *et al.* Intracellular uptake of macromolecules by brain lymphatic endothelial cells during zebrafish embryonic development. *Elife* **6**, doi:10.7554/eLife.25932 (2017).

30 Venero Galanternik, M. *et al.* A novel perivascular cell population in the zebrafish brain. *Elife* **6**, doi:10.7554/eLife.24369 (2017).

31 Kuchler, A. M. *et al.* Development of the zebrafish lymphatic system requires VEGFC signaling. *Curr Biol* **16**, 1244-1248, doi:10.1016/j.cub.2006.05.026 (2006).

32 Hogan, B. M. & Schulte-Merker, S. How to Plumb a Pisces: Understanding Vascular Development and Disease Using Zebrafish Embryos. *Dev Cell* **42**, 567-583, doi:10.1016/j.devcel.2017.08.015 (2017).

33 He, Z., Brazovskaja, A., Ebert, S., Camp, J. G. & Treutlein, B. CSS: cluster similarity spectrum integration of single-cell genomics data. *Genome Biol* **21**, 224, doi:10.1186/s13059-020-02147-4 (2020).

34 Stuart, T. *et al.* Comprehensive Integration of Single-Cell Data. *Cell* **177**, 1888-1902 e1821, doi:10.1016/j.cell.2019.05.031 (2019).

35 Becht, E. *et al.* Dimensionality reduction for visualizing single-cell data using UMAP. *Nat Biotechnol*, doi:10.1038/nbt.4314 (2018).

36 La Manno, G. *et al.* RNA velocity of single cells. *Nature* **560**, 494-498, doi:10.1038/s41586-018-0414-6 (2018).
37 Thomas, P. D. *et al.* Applications for protein sequence-function evolution data: mRNA/protein expression analysis and coding SNP scoring tools. *Nucleic Acids Res* **34**, W645-650, doi:10.1093/nar/gkl229 (2006).
38 Wigle, J. T. *et al.* An essential role for Prox1 in the induction of the lymphatic endothelial cell phenotype. *EMBO J* **21**, 1505-1513, doi:10.1093/emboj/21.7.1505 (2002).
39 Kang, J. *et al.* An exquisite cross-control mechanism among endothelial cell fate regulators directs the plasticity and heterogeneity of lymphatic endothelial cells. *Blood* **116**, 140-150, doi:10.1182/blood-2009-11-252270 (2010).
40 Jerafi-Vider, A. *et al.* VEGFC/FLT4-induced cell-cycle arrest mediates sprouting and differentiation of venous and lymphatic endothelial cells. *Cell Rep* **35**, 109255, doi:10.1016/j.celrep.2021.109255 (2021).
41 Koltowska, K. *et al.* The RNA helicase Ddx21 controls Vegfc-driven developmental lymphangiogenesis by balancing endothelial cell ribosome biogenesis and p53 function. *Nat Cell Biol* **23**, 1136-1147, doi:10.1038/s41556-021-00784-w (2021).
42 Burrows, P. E. *et al.* Lymphatic abnormalities are associated with RASA1 gene mutations in mouse and man. *Proc Natl Acad Sci U S A* **110**, 8621-8626, doi:10.1073/pnas.1222722110 (2013).
43 Frye, M. *et al.* EphrinB2-EphB4 signalling provides Rho-mediated homeostatic control of lymphatic endothelial cell junction integrity. *Elife* **9**, doi:10.7554/eLife.57732 (2020).
44 Geng, X. *et al.* S1PR1 regulates the quiescence of lymphatic vessels by inhibiting laminar shear stress-dependent VEGF-C signaling. *JCI Insight* **5**, doi:10.1172/jci.insight.137652 (2020).
45 Grimm, L. *et al.* Yap1 promotes sprouting and proliferation of lymphatic progenitors downstream of Vegfc in the zebrafish trunk. *Elife* **8**, doi:10.7554/eLife.42881 (2019).
46 Koltowska, K. *et al.* mafba is a downstream transcriptional effector of Vegfc signaling essential for embryonic lymphangiogenesis in zebrafish. *Genes Dev* **29**, 1618-1630, doi:10.1101/gad.263210.115 (2015).
47 Yuan, L. *et al.* Abnormal lymphatic vessel development in neuropilin 2 mutant mice. *Development* **129**, 4797-4806 (2002).
48 Termini, C. M. & Gillette, J. M. Tetraspanins Function as Regulators of Cellular Signaling. *Front Cell Dev Biol* **5**, 34, doi:10.3389/fcell.2017.00034 (2017).
49 Wu, R. S. *et al.* A Rapid Method for Directed Gene Knockout for Screening in G0 Zebrafish. *Dev Cell* **46**, 112-125 e114, doi:10.1016/j.devcel.2018.06.003 (2018).
50 Armour, S. M. *et al.* An HDAC3-PROX1 corepressor module acts on HNF4alpha to control hepatic triglycerides. *Nat Commun* **8**, 549, doi:10.1038/s41467-017-00772-5 (2017).
51 Liu, X. *et al.* Mitotic Implantation of the Transcription Factor Prospero via Phase Separation Drives Terminal Neuronal Differentiation. *Dev Cell* **52**, 277-293 e278, doi:10.1016/j.devcel.2019.11.019 (2020).
52 Qin, J. *et al.* Prospero-related homeobox (Prox1) is a corepressor of human liver receptor homolog-1 and suppresses the transcription of the cholesterol 7-alpha-hydroxylase gene. *Mol Endocrinol* **18**, 2424-2439, doi:10.1210/me.2004-0009 (2004).
53 Song, K. H., Li, T. & Chiang, J. Y. A Prospero-related homeodomain protein is a novel co-regulator of hepatocyte nuclear factor 4alpha that regulates the cholesterol 7alpha-hydroxylase gene. *J Biol Chem* **281**, 10081-10088, doi:10.1074/jbc.M513420200 (2006).

1182 54 Takeda, Y. & Jetten, A. M. Prospero-related homeobox 1 (Prox1) functions as a novel
1183 modulator of retinoic acid-related orphan receptors alpha- and gamma-mediated
1184 transactivation. *Nucleic Acids Res* **41**, 6992-7008, doi:10.1093/nar/gkt447 (2013).
1185 55 Lawson, N. D. & Weinstein, B. M. In vivo imaging of embryonic vascular
1186 development using transgenic zebrafish. *Dev Biol* **248**, 307-318,
1187 doi:10.1006/dbio.2002.0711 (2002).
1188 56 Ciruna, B. *et al.* Production of maternal-zygotic mutant zebrafish by germ-line
1189 replacement. *Proc Natl Acad Sci U S A* **99**, 14919-14924,
1190 doi:10.1073/pnas.222459999 (2002).
1191 57 Westerfield, M. *The Zebrafish Book. A Guide for the Laboratory use of Zebrafish*
1192 *(Danio rerio)*. 4 edn, (University of Oregorn Press, 2000).
1193 58 Gagnon, J. A. *et al.* Efficient mutagenesis by Cas9 protein-mediated oligonucleotide
1194 insertion and large-scale assessment of single-guide RNAs. *PLoS One* **9**, e98186,
1195 doi:10.1371/journal.pone.0098186 (2014).
1196 59 Bussmann, J. & Schulte-Merker, S. Rapid BAC selection for tol2-mediated
1197 transgenesis in zebrafish. *Development* **138**, 4327-4332, doi:10.1242/dev.068080
1198 (2011).
1199 60 Okuda, K. S., Baek, S. & Hogan, B. M. Visualization and Tools for Analysis of
1200 Zebrafish Lymphatic Development. *Methods Mol Biol* **1846**, 55-70, doi:10.1007/978-
1201 1-4939-8712-2_4 (2018).
1202 61 Bower, N. I. *et al.* Vegfd modulates both angiogenesis and lymphangiogenesis during
1203 zebrafish embryonic development. *Development* **144**, 507-518,
1204 doi:10.1242/dev.146969 (2017).
1205 62 Kartopawiro, J. *et al.* Arap3 is dysregulated in a mouse model of hypotrichosis-
1206 lymphedema-telangiectasia and regulates lymphatic vascular development. *Hum Mol*
1207 *Genet* **23**, 1286-1297, doi:10.1093/hmg/ddt518 (2014).
1208 63 Zheng, G. X. *et al.* Massively parallel digital transcriptional profiling of single cells.
1209 *Nat Commun* **8**, 14049, doi:10.1038/ncomms14049 (2017).
1210 64 Wolock, S. L., Lopez, R. & Klein, A. M. Scrublet: Computational Identification of
1211 Cell Doublets in Single-Cell Transcriptomic Data. *Cell Syst* **8**, 281-291 e289,
1212 doi:10.1016/j.cels.2018.11.005 (2019).
1213 65 Butler, A., Hoffman, P., Smibert, P., Papalexi, E. & Satija, R. Integrating single-cell
1214 transcriptomic data across different conditions, technologies, and species. *Nat*
1215 *Biotechnol* **36**, 411-420, doi:10.1038/nbt.4096 (2018).
1216 66 McCarthy, D. J., Campbell, K. R., Lun, A. T. & Wills, Q. F. Scater: pre-processing,
1217 quality control, normalization and visualization of single-cell RNA-seq data in R.
1218 *Bioinformatics* **33**, 1179-1186, doi:10.1093/bioinformatics/btw777 (2017).
1219 67 Zappia, L. & Oshlack, A. Clustering trees: a visualization for evaluating clusterings at
1220 multiple resolutions. *Gigascience* **7**, doi:10.1093/gigascience/giy083 (2018).
1221 68 Kejie Li, Z. O., Dongdong Lin, Michael Mingueneau, Will Chen, David Sexton,
1222 Baohong Zhang. cellxgene VIP unleashes full power of interactive visualization,
1223 plotting and analysis of scRNA-seq data in the scale of millions of cells. *bioRxiv*
1224 **2020.08.28.270652**, doi:https://doi.org/10.1101/2020.08.28.270652 (2020).
1225 69 Kazenwadel, J. *et al.* GATA2 is required for lymphatic vessel valve development and
1226 maintenance. *J Clin Invest* **125**, 2979-2994, doi:10.1172/JCI78888 (2015).
1227 70 Li, H. & Durbin, R. Fast and accurate short read alignment with Burrows-Wheeler
1228 transform. *Bioinformatics* **25**, 1754-1760, doi:10.1093/bioinformatics/btp324 (2009).
1229 71 Quinlan, A. R. & Hall, I. M. BEDTools: a flexible suite of utilities for comparing
1230 genomic features. *Bioinformatics* **26**, 841-842, doi:10.1093/bioinformatics/btq033
1231 (2010).